JCI The Journal of Clinical Investigation

CERT1 mutations perturb human development by disrupting sphingolipid homeostasis

Charlotte Gehin, … , Giovanni D'Angelo, Vincenzo A Gennarino

J Clin Invest. 2023. https://doi.org/10.1172/JCI165019.

Research In-Press Preview Cell biology Genetics

Graphical abstract

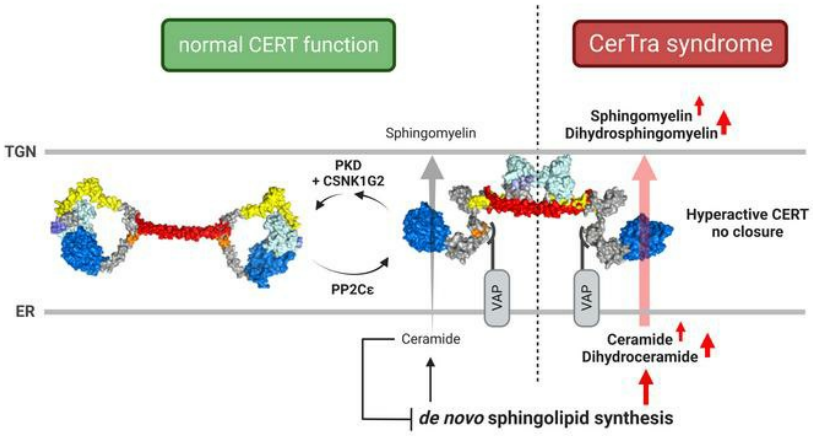

Find the latest version:

https://jci.me/165019/pdf

CERT1 mutations perturb human development by disrupting sphingolipid homeostasis

Charlotte Gehin[1]*, Museer A. Lone[2]*, Winston Lee[3,4]*, Laura Capolupo[1]*, Sylvia Ho[1], Adekemi M. Adeyemi[5], Erica H. Gerkes[6], Alexander P.A. Stegmann[7], Estrella López-Martín[8], Eva Bermejo-Sánchez[8], Beatriz Martínez-Delgado[8], Christiane Zweier[9,10], Cornelia Kraus[9], Bernt Popp[11,12], Vincent Strehlow[11], Daniel Gräfe[13], Ina Knerr[14,15], Eppie R. Jones[16], Stefano Zamuner[17], Luciano A. Abriata[18], Vidya Kunnathully[19], Brandon E. Moeller[20], Anthony Vocat[1], Samuel Rommelaere[21], Jean-Philippe Bocquete[21], Evelyne Ruchti[22], Greta Limoni[22], Marine Van Campenhoudt[22], Samuel Bourgeat[22], Petra Henklein[23], Christian Gilissen[24,25], Bregje W. van Bon[24], Rolph Pfundt[24,25], Marjolein H. Willemsen[24], Jolanda H. Schieving[26], Emanuela Leonardi[27,28], Fiorenza Soli[29], Alessandra Murgia[28], Hui Guo[30], Qiumeng Zhang[30], Kun Xia[30], Christina R. Fagerberg[31], Christoph P. Beier[31], Martin J. Larsen[31], Irene Valenzuela[32], Paula Fernández-Álvarez[32], Shiyi Xiong[33], Robert Śmigiel[34], Vanesa López-González[35], Lluís Armengol[36], Manuela Morleo[37,38], Angelo Selicorni[39], Annalaura Torella[37,38], Moira Blyth[40], Nicola S. Cooper[41], Valerie Wilson[42], Renske Oegema[43], Yvan Herenger[44], Aurore Garde[45,46], Ange-Line Bruel[46,47], Frederic Tran Mau-Them[46,47], Alexis B.R. Maddocks[48], Jennifer M. Bain[49], Musadiq A. Bhat[50], Gregory Costain[51], Peter Kannu[52], Ashish Marwaha[5], Neena L. Champaigne[53], Michael J. Friez[53], Ellen B Richardson[53], Vykuntaraju K. Gowda[54], Varunvenkat M. Srinivasan[54], Yask Gupta[55], Tze Y. Lim[55], Simone Sanna-Cherchi[55], Bruno Lemaitre[21], Toshiyuki Yamaji[56], Kentaro Hanada[56], John E. Burke[20,57], Ana Marjia Jaksic[22], Brian D. McCabe[22], Paolo De Los Rios[1,17], Thorsten Hornemann[2,†], Giovanni D'Angelo[1,19,21†], and Vincenzo A. Gennarino[3,58,59,60,61,†].

[1] Institute of Bioengineering (IBI), École Polytechnique Fédérale de Lausanne (EPFL), Lausanne, Switzerland. [2]Institute of Clinical Chemistry, University Hospital Zurich, University of Zurich, Zurich, Switzerland. [3]Department of Genetics and Development, Columbia University Irving Medical Center, New York, NY. [4]Department Ophthalmology, Columbia University Irving Medical Center, New York, NY. [5]Department of Medical Genetics, Cumming school of medicine, The University of Calgary. [6]University of Groningen, University Medical Center Groningen, Department of Genetics, Groningen, The Netherlands. [7]Department of Clinical Genetics and School for Oncology & Developmental Biology (GROW), Maastricht University Medical Center, Maastricht, The Netherlands. [8]Institute of Rare Diseases Research (IIER), Instituto de Salud Carlos III, 28029 Madrid, Spain. [9]Institute of Human Genetics, Friedrich-Alexander-Universität Erlangen-Nürnberg, Schwabachanlage 10, 91054 Erlangen, Germany. [10]Department of Human Genetics, Inselspital, Bern University Hospital, University of Bern, Freiburgstrasse 15, 3010 Bern, Switzerland.[11]Institute of Human Genetics, University of Leipzig Medical Center, Leipzig, Germany. [12]Berlin Institute of Health at Charité - Universitätsmedizin Berlin, Center of

Functional Genomics, Hessische Straße 4A, 10115 Berlin, Germany. [13]Department of Pediatric Radiology, University Hospital Leipzig, Leipzig. 20a, 04103 Leipzig, Germany. [14]National Centre for Inherited Metabolic Disorders, Children's Health Ireland (CHI) at Temple Street, Dublin, Ireland. [15]UCD School of Medicine, Dublin, Ireland. [16]Genuity Science, Cherrywood Business Park, Dublin, Ireland. [17]Institute of Physics, School of Basic Sciences, École Polytechnique Féderale de Lausanne (EPFL), Lausanne, Switzerland. [18]Laboratory for Biomolecular Modeling & Protein Purification and Structure Facility, École Polytechnique Fédérale de Lausanne (EPFL) and Swiss Institute of Bioinformatics, Switzerland. [19]Institute of Biochemistry and Cell Biology, National Research Council, Naples, Italy. [20]Department of Biochemistry and Microbiology, University of Victoria, Victoria, Canada. [21]Global Health Institute, School of Life Sciences, École Polytechnique Féderale de Lausanne (EPFL), Lausanne, Switzerland. [22]Brain Mind Institute, School of Life Sciences, École Polytechnique Féderale de Lausanne (EPFL), Lausanne, Switzerland. [23]Berlin Institute of Health, Institut für Biochemie, Charité-Universitätsmedizin Berlin, Corporate Member of Freie Universität Berlin, Humboldt-Universität zu Berlin, Berlin, Germany. [24]Radboud University Medical Center, Department of Human Genetics, P.O. box, 6500 HB Nijmegen (836), The Netherlands. [25]Radboud Institute for Molecular Life Sciences, 6525GA Nijmegen, the Netherlands. [26]Radboud University Medical Center, Department of Pediatric Neurology, Amalia Children's Hospital and Donders Institute for Brain, Cognition and Behavior, Nijmegen, The Netherlands. [27]Molecular Genetics of Neurodevelopment, Dept. of Woman and Child Health, University of Padova, Padova, Italy. [28]Fondazione Istituto di Ricerca Pediatrica (IRP), Città della Speranza, Padova, Italy. [29]Medical Genetics Department, APSS Trento, Trento, Italy. [30]Center for Medical Genetics & Hunan Key Laboratory of Medical Genetics, School of Life Sciences, Central South University, Changsha, Hunan, China. [31]Department of Neurology, Odense University Hospital, and Department of Clinical Research, University of Southern Denmark Sdr. Boulevard 29, 5000 Odense C. [32]Department of Clinical and Molecular Genetics, University Hospital Vall d´Hebron; Medicine Genetics Group, Valle Hebron Research Institute, Barcelona, Spain. [33]Fetal Medicine Unit & Prenatal diagnosis center, Shanghai First Maternity and Infant Hospital, Tongji University School of Medicine, Shanghai, People's Republic of China. [34]Department of Family and Pediatric Nursing, Medical University, Bartla 5, 51-618 Wroclaw, Poland. [35]Sección de Genética Médica, Servicio de Pediatría, Hospital Clínico Universitario Virgen de la Arrixaca, IMIB-Arrixaca, CIBERER-ISCIII, Murcia, Spain. [36]Quantitative Genomic Medicine Laboratories, S.L., CSO & CEO, Joan XXIII, 10, 08950 Esplugues del Llobregat, Barcelona – Catalunya, Spain. [37]Telethon Institute of Genetics and Medicine (TIGEM), Pozzuoli, Naples, Italy. [38]Department of Precision Medicine, University of Campania "Luigi Vanvitelli", Naples, Italy. [39]Department of Pediatrics, ASST Lariana Sant' Anna Hospital, San Fermo Della Battaglia, Como, Italy. [40]North of Scotland Regional Genetics Service, Clinical Genetics Centre, Ashgrove House, Foresterhill, Aberdeen, AB25 2ZA, UK.

[41]W Midlands Clinical Genetics Service, Birmingham Women's Hospital, Metchley Park Road, Edgbaston Birmingham, UK. [42]Northern Regional Genetics Laboratory, Newcastle upon Tyne, UK. [43]Department of Genetics, University Medical Center Utrecht, Utrecht University, Utrecht, the Netherlands. [44]Genetica AG, Humangenetisches Labor und Beratungsstelle, Weinbergstrasse 9, 8001 Zürich, Switzerland. [45]Centre de Référence Anomalies du Développement et Syndromes Malformatifs, FHU TRANSLAD, Hôpital d'Enfants, CHU Dijon, Dijon, France. [46]UMR1231 GAD, Inserm - Université Bourgogne-Franche Comté, Dijon, France. [47]Unité Fonctionnelle Innovation en Diagnostic génomique des maladies rares, FHU-TRANSLAD, CHU Dijon Bourgogne, Dijon, France. [48]Department of Radiology at Columbia University Irving Medical Center New York, NY. [49]Department of Neurology, Columbia University Irving Medical Center; New York Presbyterian Hospital, Columbia University Medical Center, New York, NY. [50]Institute of Pharmacology and Toxicology University of Zürich, Winterthurerstrasse-190, Zürich-8057. [51]Division of Clinical and Metabolic Genetics, The Hospital for Sick Children, Toronto, ON, Canada. [52]Department of Medical Genetics, University of Alberta. [53]Greenwood Genetic Center and the Medical University of South Carolina. [54]Department of pediatric neurology, Indira Gandhi institute of child health, Bangalore, India. [55]Division of Nephrology, Department of Medicine, Columbia University, New York, NY, USA. [56]Department of Biochemistry & Cell Biology, National Institute of Infectious Diseases, Tokyo, Japan. [57]Department of Biochemistry and Molecular Biology, The University of British Columbia, Vancouver, BC, Canada. [58]Department of Pediatrics, Columbia University Irving Medical Center, New York, NY. [59]Department of and Neurology, Columbia University Irving Medical Center, New York, NY. [60]Columbia Stem Cell Initiative, Columbia University Irving Medical Center, New York, NY. [61]Initiative for Columbia Ataxia and Tremor, Columbia University Irving Medical Center, New York, NY.

*These authors contributed to the manuscript equally.

†Co-corresponding authors:
Thorsten Hornemann, Clinical Chemistry (IKC), USZ WAGI, Wagistrasse 14, CH-8952 Schlieren, Switzerland; Phone: +41 44 556 3101; thorsten.hornemann@usz.ch.
Giovanni D'Angelo, EPFL, SV/IBI/UPDANGELO, Station 19, CH-1015 Lausanne, Switzerland; Phone: +41 21 693 4276; giovanni.dangelo@epfl.ch.
Vincenzo A. Gennarino, Department of Genetics & Development (CUIMC), 701 West 168th Street, HHSC 1402, New York, 10032 New York, USA; Phone: +1 212 305 7863; vag2138@cumc.columbia.edu.
These authors co-supervised the project.

Abstract

Neural differentiation, synaptic transmission, and action potential propagation depend on membrane sphingolipids, whose metabolism is tightly regulated. Mutations in the ceramide transporter CERT (*CERT1*), which is involved in sphingolipid biosynthesis, are associated with intellectual disability, but the pathogenic mechanism remains obscure. Here, we characterize 31 individuals with *de novo* missense variants in *CERT1*. Several variants fall into a previously uncharacterized dimeric helical domain that enables CERT homeostatic inactivation, without which sphingolipid production goes unchecked. The clinical severity reflects the degree to which CERT autoregulation is disrupted, and inhibiting CERT pharmacologically corrects morphological and motor abnormalities in a *Drosophila* model of the disease, which we call CerTra syndrome. These findings uncover a central role for CERT autoregulation in the control of the sphingolipid biosynthetic flux, provide unexpected insight into the structural organisation of CERT, and suggest a possible therapeutic approach for CerTra syndrome patients.

Introduction

Sphingolipids play numerous essential roles in membrane structure, signal transduction, and brain development and function (1-3). The central nervous system is particularly affected by disturbances in sphingolipid production or clearance: defective production can cause hereditary sensory neuropathy, spastic paraplegia, or infantile epilepsy syndrome, whereas toxic accumulation of sphingolipids underlies a number of devastating inborn errors of metabolism such as Gaucher disease, Farber disease, Niemann-Pick type A, Krabbe, Tay-Sachs, and Sandhoff diseases (1, 4). Sphingolipid metabolic fluxes therefore must be tightly regulated through homeostatic circuits (5). A key checkpoint in sphingolipid biosynthesis occurs at contact sites between the endoplasmic reticulum (ER) and the *trans* Golgi membrane, where the Ceramide Transporter (CERT) transfers ceramide (Cer) from the ER to the *trans* Golgi for its conversion to sphingomyelin (SM) (6). When sufficient rates of SM production are reached, CERT is phosphorylated and undergoes a conformational change that renders it inactive (7).

Given the central position of CERT in sphingolipid metabolism, its malfunction should be detrimental to human health, and particularly to neural function. Thus far, one case report and several case-control screening studies have described associations between variants in *CERT1* (ceramide transporter 1), the gene that encodes CERT, and neurological abnormalities (8-16). Nonetheless, there has not been a systematic assessment of the mutational landscape of *CERT1* in humans, and whether or how *CERT1* mutations cause neurological disease remains to be proven.

In this study, we characterised 31 unrelated individuals with 22 distinct missense variants in *CERT1*, 18 of which have not been previously reported. These patients have a syndromic presentation characterised by infantile hypotonia; mild dysmorphologies (affecting the face, hands or feet); variable

degrees of intellectual disability, motor and speech delays; increased pain tolerance; and seizures. We investigated the effect of CerTra mutations on CERT function, regulation, and structure. We found that several CerTra mutations disrupt CERT autoregulation, leading to a gain in CERT activity, increased *de novo* sphingolipid synthesis in the ER, and skewed metabolic flux towards the production of potentially neurotoxic compounds. We found that CERT gain of function in *Drosophila melanogaster* led to head and brain size defects and to impaired locomotor activity, which we corrected by pharmacological inhibition of CERT. Biochemical characterization of disease-causing *CERT1* mutations led us to identify an unanticipated structured region within CERT that is essential to its autoregulation and to sphingolipid homeostasis.

Results

Characterization of CERT1-associated phenotypes

Most of the *CERT1* variants reported so far have been associated with intellectual disability (13) (Figure 1A, and Supplemental Table 1), but the clinical phenotype has been characterized for only one of these individuals, who bears an S135P variant (13). We therefore sought *CERT1* mutation carriers from multiple international disease consortia and databases (see Methods and Supplemental Methods). We identified 50 patients who carry a potentially pathogenic variant in *CERT1* (45 in the coding sequence; hg19:NM_005713.3, Figure 1A, and Supplemental Table 1 and 2) (17). We obtained thorough clinical histories for 31 patients: 27 from the present cohort, three who were initially included in genetic screening consortia for intellectual disability (8, 10, 12), and the patient who had been characterized clinically (13) (Supplemental Table 2-3, and Supplemental Clinical Appendix for each subject). Family segregation confirmed that *CERT1* variants occurred *de novo* in 93% (25/27) of cases. Biparental samples were not available for Subjects [S] 1, 19, 20, or 24 (see Supplementary Clinical Appendix). The p.V326F variant in S21 was inherited from her reportedly unaffected father, whereas the p.A449V variant in S26 was inherited from her mother, who was diagnosed with intellectual disability (Supplemental Table 2 and Supplemental Clinical Appendix).

The detailed clinical information we were able to gather (see Supplemental Clinical Appendix and Supplemental Table 2) revealed cognitive, motor, and speech delays of variable degrees of severity. Of the subjects for whom we had birth information, only four were of average weight at birth; most were born slightly to significantly underweight. Similarly, only four of the subjects did not present some form of developmental delay by the end of the first year of life (4/26, 15%), with the latest onset being at age four (Figure 1A-C). Fifteen (out of 24) had neonatal feeding difficulties, often with hypotonia or failure to thrive. These were likely early manifestations of what would later become frank motor delays, affecting 26 out of 29 subjects (Figure 1B). Intellectual disability ranged from mild to profound, as per the criteria

of the DSM-V (18) (see Methods); the latter subjects are nonverbal, lack age-appropriate daily living skills and require safety supervision. Neurobehavioral abnormalities frequently led to a diagnosis of autism spectrum disorder (ASD) (19/27, 70%); some patients displayed stereotypic hand movements (14/18), self-injurious behaviour (9/19), high pain tolerance (9/18), disrupted sleep patterns (9/21), attention deficit-hyperactivity disorder (10/19), or aggression (6/20). Multiple seizure types were reported (16/29). Neuroimaging frequently revealed a thin corpus callosum, ventriculomegaly, delayed myelination, and cerebellar atrophy (Supplemental Figure 1B).

Subtle facial dysmorphisms included anteverted nares with depressed or broad nasal bridge, enlarged earlobes, synophrys, micrognathia, dental anomalies (protruding incisors and diastema), and palatine ridges (Supplemental Figure 1A, and, Supplemental Figure 2A-E). Anomalies affecting the hands, feet, or digits included 3rd/4th finger syndactyly, club foot, or hallux varus (sandal gaps); the first metatarsal also tended to be short, while the fifth fingers tended to be long (Supplemental Figure 2F).

The majority (27/31, 87%) of variants from our enrolled patients occurred in the region between the PH and START domains (Figure 1A), as was the case for previously reported variants (13). These variants populated four distinct sub-regions whereby the geometric mean distance (δg) between variants within each spatial group indicated a greater likelihood of clustering compared to random permutations (Figure 1A). (Note that human *CERT1* produces at least two splicing variants that are both widely expressed (13). In this report we have used *CERT1* isoform 1 (also known as $CERT_L$) for both amino acid numbering and overexpression/structural experiments).

The first four serine residues of the SRR (132-SMVSLVSGASGYSATSTSS-150) are hotspots for mutations (Cluster 1): p.S132 (n=7; four enrolled), p.S135 (n=4; two enrolled), p.S138 (n=4; two enrolled), p.S141 (n=1; one enrolled) (Figure 1B). An alanine substitution at p.T166 was found in five subjects in our cohort (four enrolled; Cluster 2). Between residues 240 to 254 (Cluster 3), missense variants were found at p.D240 (n=1), p.G243 (n=4, four enrolled), p.T247 (n=1, one enrolled), and p.T251 (n=1, one enrolled). Four variants p.V326F, p.A329P, p.L330V, and p.L330P are located at the C-terminal end of the CERT FFAT motif (Cluster 4).

For the variants that recurred in multiple subjects, we were able to sketch out broad genotype-phenotype correlations. The most severe phenotypes—with congenital or perinatal onset, profound to severe intellectual disability, and the greatest motor delay—resulted from mutations at p.S132 and p.S135 (Figure 1B, C and Table 1). Subjects bearing mutations at p.S138, p.T166, or p.G243 tended to not have perinatal difficulties and achieved early developmental milestones (S8 did not show difficulties until 4 years of age) but then regressed or slowed in their development. Seizures likely contribute to the developmental delays: neither subject with a p.S138C mutation had seizures and have only moderate ID, but S13, the most severely affected of the p.T166A carriers, has an epileptic

encephalopathy that apparently halted her development at 19 months. All variants associated with more severe phenotypes were predicted to be deleterious by CADDv1.6, REVEL, M-CAP, and Eigen (Supplemental Table 4). Approximately half of the variants among the more moderately affected had inconsistent pathogenicity predictions across algorithms. On average, variants among patients had significantly greater CADDv1.6, M-CAP, REVEL and Eigen pathogenicity scores than gnomAD singleton missense variants ($P<0.001$, Mann-Whitney U-test).

Variants p.D59E (15), T166A (19) and F182L (9) were previously identified in ASD cohorts (Supplemental Table 1). To determine the extent to which *CERT1* mutations contribute to autism, we conducted a targeted *de novo* analysis interrogating the Simons Foundation Powering Autism Research (SPARK) initiative database, which includes genomic data from nearly 35,000 ASD individuals (See Supplemental Methods). No *de novo* protein-altering variants were observed in the Simons exome cohort. Denovo-db (v.1.6.1) confirmed the negative findings for the exome cohort but identified one *de novo* genome missense mutation (pos=74721285, T>C, c.880A>G, p.(T294A), exon6) in one of 516 trios. This analysis, along with the fact that none of the subjects in our cohort was diagnosed with ASD as a primary condition, indicates that *CERT1* variants are unlikely to be a significant contributor to autism but instead cause a recognizable neurodevelopmental syndrome distinct from ASD, which we will refer to as **Cer**amide **Tra**nsporter (CerTra) syndrome.

CerTra mutations disrupt CERT regulation

CERT oscillates between cytosolic and membrane-associated forms (20), according to its activation state in the homeostatic cycle (7). Active, membrane-associated CERT provides Cer to sphingomyelin synthase 1 for its conversion to SM with concomitant production of diacylglycerol. The diacylglycerol produced in the sphingomyelin synthase 1 reaction triggers a signalling response involving the recruitment of PKD (protein kinase D) to the *trans* Golgi (21-23). PKD initiates CERT phosphorylation at p.S132 (7); CSNK1G2 (casein kinase 1 gamma 1) then phosphorylates the rest of the SRR phosphosites (24-27). Following phosphorylation, CERT undergoes a conformational change that leads to its cytosolic redistribution and inactivation (20, 26, 28); all this can then be reversed by the action of the ER phosphatase PP2Cε (protein phosphatase 2C epsilon) (29). Mutations leading to abnormally activated CERT redistribute the protein to Golgi membranes and cytosolic spots, while inactivating mutations redistribute it to the cytosol (30, 31).

To determine whether disease-causing variants alter CERT localization, we used automated microscopy to capture GFP-tagged WT and CerTra-associated CERT variants in transfected HeLa cells (see Supplemental Methods). Eighteen of the 22 CERT mutants exhibited a greater tendency than WT to associate with the perinuclear membranes and cytosolic spots (Figure 2A, and B). These included all

variants mapping to Clusters 1 to 4 (Figure 1B), those located between Clusters 3 and 4, the S93R in the PH domain and the P500L in the START domain. A similar phenotype was observed in patient-derived fibroblasts bearing the p.G243R mutation (Supplemental Figure 3A, and B). Four consecutive variants (R366T, I382V, E424G, A449V) did not show a different distribution from CERT WT.

We next evaluated the phosphorylation pattern of CERT WT and mutants by SDS-PAGE (Figure 2C). Wild-type CERT migrates on SDS gels as a doublet, with the fast- and slow-migrating bands corresponding to the active/hypophosphorylated and the inactive/hyperphosphorylated forms of CERT, respectively (24). By contrast, all variants belonging to Clusters 1, 2, and 3 showed hypo-phosphorylation, while mutations outside of these clusters did not. Mass spectrometry-based assessment of selected variants belonging to Clusters 1, 2 , and 3 showed that these *CERT1* mutations did not affect CERT phosphorylation outside the SRR or SRR mono-phosphorylation (likely on p.S132), and suggest that CSNK1G2 mediated SSR phosphorylation is defective in these mutants (Supplemental Figure 3D).

Although we expected hypo-phosphorylation and increased membrane recruitment for CERT mutants within the SRR (Cluster 1) (13, 27), this was not intuitive for Clusters 2 and 3. We therefore investigated the regulation of the two most frequent *CERT1* mutations in these Clusters, p.G243R, for which some biochemical characterisation was already reported (30), and p.T166A. These two variants were effectively phosphorylated at p.S132 by PKD in both in vitro and cell-based assays (Supplemental Figure 3D, and E). Moreover, the p.S132 phospho-mimetic mutant (HGS 130-132 DDD) (27) in the p.G243R and p.T166A backgrounds did not differ in either localization or SDS-PAGE migration (Supplemental Figure 3F-H). This supports the idea that the Cluster 2 and 3 mutations affect CERT regulation downstream of PKD phosphorylation. To test this possibility, we co-expressed CSNK1G2 or PP2Cε with the hypo-phosphorylated CERT mutants. Overexpression of CSNK1G2 led to reduced membrane association of most mutants (p.S132L served as a negative control; Figure 3A-C), indicating that these can be phosphorylated and inactivated by CSNK1G2. Interestingly, although PP2Cε overexpression had little effect on WT CERT phosphorylation or localization, consistent with previous results (27), hypo-phosphorylated CERT mutants were sensitive to PP2Cε overexpression (Figure 3A-C).

Thus, CerTra-associated *CERT1* mutations generally disturb CERT regulation and promote its membrane association. Mutations in Clusters 1, 2, and 3 also reduce the pool of hyperphosphorylated/ inactive CERT by influencing the CERT phosphorylation cycle that depends on the consecutive action of PKD and CSNK1G2 kinases and on the PP2Cε phosphatase.

CerTra mutations disrupt sphingolipid homeostasis

Sphingolipid biosynthesis starts at the ER with the generation of Cer (32-34). Cer is then transported to the Golgi complex by vesicular carriers for the production of glucosylceramide and downstream glycosphingolipids, or transferred directly to the *trans* Golgi by CERT for its conversion to SM (6) (Figure 3A).

We profiled sphingolipids in *CERT1*-deficient (*CERT1*-KO) HeLa cells expressing six CERT mutants tagged with GFP. *CERT1* KO causes a defect in Cer to SM conversion (35) that is expected to be reverted by the expression of active CERT. Overexpression of CERT WT in *CERT1*-KO cells, in fact, induced a five-fold increase of SM levels coupled to an unexpected increase in Cer and complex glycosphingolipids (Figure 3B, and Supplemental Figure 4A). Overexpression of CERT mutants also increased SM and Cer levels but significantly reduced glycosphingolipid levels compared to WT. Unexpectedly, CERT overexpression increased dihydro-ceramide (dhCer) and dihydro-sphingomyelin (dhSM), and this was even more pronounced with mutant overexpression (Figure 3B, and Supplemental Figure 4A). Variants associated with more severe manifestations in patients (i.e., at p.S132, p.S135, and p.G243) were associated with the greatest increases.

We observed that *CERT1* overexpression produces an overall increase in sphingolipid levels (Figure 3B). To determine whether this was due to increased synthesis, decreased catabolism, or both, we used a D_3-^{15}N-Serine labelling approach (see Methods). Lipids were extracted and subjected to chemical hydrolysis to release long chain bases from sphingolipids and dihydro-sphingolipids. These long chain bases reflect total levels of steady-state and newly synthesised sphingolipids, represented by sphingosine (SO) and sphingosine+3 (SO+3), respectively, while steady-state and newly synthesised dihydro-sphingolipids are represented by sphinganine (SA) and sphinganine+3 (SA+3), respectively. Overexpression of CERT mutants had little effect on SO but increased SO+3 by 200%. All mutants had twice the amount of SA compared to CERT WT, but SA+3 levels rose at least 300% in the case of the mildest mutant, p.T166A, and considerably more for the other mutants (Figure 3C).

These data indicate that CERT activity promotes *de novo* sphingolipid production, possibly by relaxing the Cer-dependent inhibition of serine palmitoyltransferase (SPT) (36) (Supplemental Figure 5A). To test this hypothesis, we repeated our metabolic labelling experiment in parental and *CERT1*-KO HeLa cells treated with N-[(1R,3S)-3-hydroxy-1-(hydroxymethyl)-3-phenylpropyl]-dodecanamide (HPA-12, a CERT inhibitor) (37) or, as a control, with myriocin (Myr), an inhibitor of SPT and therefore of sphingolipid production (Supplemental Figure 4A). Treatment with HPA-12 reduced sphingolipid synthesis more than 80% (similar to what was obtained by treating cells with Myr) in HeLa cells but had no effect in *CERT1*-KO cells where sphingolipid synthesis was already greatly reduced (Supplemental Figure 5B).

The metabolic alterations induced by overexpressing *CERT1* mutants in *CERT1*-KO cells were confirmed in patient-derived fibroblasts bearing the p.G243R mutation and lymphoblasts bearing the

p.T166A mutation. Patient cells produced much more dhSM and dhCer than their WT counterparts (Supplemental Figure 5C, and E). In contrast, inhibiting CERT activity with HPA-12 markedly reduced total dhCer and dhSM in both WT and patient-derived cells.

We observed a similar profile in steady-state sphingolipid levels and new synthesis when we examined patient cells after labelling with D_3-^{15}N-Serine (Supplemental Figure 5D, and F). SA+3 backbone levels were much higher in patient-derived cells than in controls. The increase in sphingolipid synthesis observed in patient cells was blocked by the administration of HPA-12, confirming that these effects are indeed caused by altered CERT activity (Supplemental Figure 4, and 5).

These data indicate that CERT activity is inherently coupled to the homeostatic regulation of *de novo* sphingolipid synthesis and suggest that frequent CerTra mutations cause an increase in CERT activity (Figure 3A).

CerTra mutations reveal an uncharacterized structural domain in CERT

The structures of the PH and START domains of CERT have been solved independently and as a complex (20, 38, 39), but little is known about the region between these two domains. It has been assumed to be largely unstructured except for a predicted coiled-coil segment that mediates CERT oligomerization upon UV irradiation (40, 41). Given the appreciable effect of CERT mutations in Clusters 2 and 3 (Figure 1C) we decided to explore their structural context. To this end, we subjected recombinant CERT to hydrogen-deuterium exchange mass spectrometry (HDX-MS), which allows the study of protein dynamics and folding by assessing the solvent accessibility of protein surfaces (42, 43).

As expected, the HDX-MS profile of CERT highlighted the presence of amides protected from H/D exchange at early time points of exchange at the N- and C-terminal regions, corresponding to the PH (aa 23-117) and START (aa 389-618) globular domains (Figure 4A, and B). The areas from amino acids 187 to 218 and from 300 to 381 were highly accessible to solvent and therefore likely either contained no or very dynamic secondary structure. Strikingly, regions encompassing Cluster 2 and 3 mutations (i.e., 152-187 and 240-300) were heavily protected from exchange, indicating secondary structure formation and/or their engagement in protein-protein interactions (i.e., CERT oligomerization).

Structural modelling based on trRosetta (44) and AlphaFold (45) predicted the existence of two helices encompassing residues 154-187 (H1) and 242-304 (H2) (Figure 4C). Coiled-coil predictors (46) also suggested the existence of a coiled-coil region spanning part of H2 (aa 263-303) (Supplemental Figure 6A). Circular dichroism confirmed that purified CERT 151-309, hereafter called the CCD (CERT Central Core Domain), and the synthetic peptides of H1 and H2 were indeed helical; the CCD has 60% helical content and a melting temperature of 43°C. (Figure 4D).

Residue coevolution calculations using direct-coupling analysis (44) on an *ad hoc* alignment support a coiled-coil arrangement of H1 and H2, but the calculations also propose pairs of contacting residues that cannot be satisfied in the monomeric model (Supplemental Figure 6B). Interestingly, native mass spectrometry (47) of the CERT CCD indicated that dimers predominate (theoretical MW 18.5 kDa, observed MW 37 kDa) (Figure 4E). When we evaluated the stoichiometry of recombinant full-length CERT with size exclusion chromatography coupled to multiangle light scattering (SEC-MALS) (48), we found the absolute molar mass of the full-length CERT molecule to be on average 142.7 kDa, which again is compatible with a dimeric form (Supplemental Figure 6C).

We therefore asked whether CERT dimerizes through its CCD domain. SEC-MALS analysis of the START domain alone (aa 389-618) indicated that it is a monomer, an oligomeric state also shared by the PH domain alone (26). By contrast, the construct encompassing the PH plus CCD domains (aa 1-341) was dimeric. Thus, although a recent study reported that CERT is organised as a homo-trimer or a higher oligomer (49), our data strongly suggest that CERT dimerizes through its CCD.

We then modelled the CCD dimer by rigid docking (see Supplemental Methods). Of the six best dimer models obtained, five had an antiparallel orientation (Supplemental Figure 6G, Supplemental Files 1-6). Antiparallel orientation was also supported by co-evolution restraints unexplained by the 3D model of the monomer (Figure 4F). However, not all predicted contacts are explained by a unique conformation, perhaps because the dimer is highly dynamic. Nonetheless, when CERT mutations were mapped onto the highest-scoring dimer model, they populated the interface between the H1 and H2 helices of the dimeric CCD, a region particularly protected from solvent as assessed by HDX-MS (Figure 4G). Here, residues p.D240, p.G243, p.T247, p.T251, and p.G254 define the side of the H2 helix that interfaces with H1 in the segment between p.T166 and p.F182, while p.Y291 and p.T296 form the H2 helix in the other CCD monomer contact the same H1 portion with a different orientation (Figure 4G).

Based on this new evidence in addition to the existing X-ray structures and the CCD model, we propose the following 3D organisation of the full-length CERT dimer: the dimer adopts a T-shaped conformation whereby the two PH domains are kept in close proximity at the extremity of the T stem, and the two START domains are at the extremities of the two T arms (Figure 4H, Supplemental File 6). Upon SRR phosphorylation, CERT undergoes a conformational change such that the PH domain first interacts with the phosphorylated SRR (26) and then forms a complex with the START domain (20). In the context of our structural model, this conformational change implies a rearrangement of the interface between H1 and H2 of the CCD, which may be impaired by CerTra mutations that map to this region (Figure 4I).

We analysed the effect of CERT mutations on the CCD structure. We evaluated the melting curves of synthetic peptides CERT 154-187 and purified CERT 151-309 WT and their mutant counterparts. We found that p.T166A decreases CERT H1 helicity and destabilises it while p.G243R has negligible effects

on CCD secondary structure and stability (Figure 4J, and Supplemental Figure 6H). Nonetheless, when we compared the HDX profile of recombinant full-length CERT WT with p.G243R, we observed diminished solvent accessibility for the p.G243R mutant in a region encompassing aa 249-256 (Figure 4K), an H2 region coordinating with H1. This suggests that, rather than impairing CCD structure, p.G243R impairs CCD dynamics and possibly its interactions with other proteins. These results suggest a model whereby the CCD enables the conformational change that takes place upon CERT phosphorylation to deactivate the protein and signal that sufficient levels of sphingomyelin production have been reached. CerTra-causing *CERT1* mutations in the CCD disturb this conformational change either by altering CCD stability (p.T166A) or CCD dynamics/ interactions (p.G243R).

CERT gain of function alters sphingolipid metabolism, brain size, and locomotion in Drosophila melanogaster

Altogether our data indicate that CerTra mutations disrupt CERT autoregulation, resulting in an inappropriate gain of CERT function and excessive sphingolipid production. To test whether this is sufficient to induce neurological manifestations in an animal model, we increased *CERT1* dosage in *D. melanogaster*. *D. melanogaster* dCERT exerts a similar metabolic activity to mammalian CERT (50) and shares 43% sequence identity with human CERT, including all six of the most recurrent CerTra variants. We generated *D. melanogaster* strains in the w^{1118} background (hereafter referred to as Control [Ctrl]) bearing two extra copies of either $dCERT^{WT}$ (hereafter +WT) or $dCERT^{p.S149L}$ (hereafter +SL; equivalent to the most common and severe CerTra mutation, p.S132L) under the control of its endogenous promoter (Figure 5A; see Supplemental Methods).

Total *dCERT* mRNA levels were 50% higher than Ctrl flies in both +WT and +SL strains, with the increase being completely ascribable to the extra exogenous copies of *dCERT* (Figure 5B). The increased gene dosage did not shorten the lifespan of transgenic *Drosophila*; in fact, both male and female animals lived slightly longer (Supplemental Figure 7A). The transgenic strains had wing and abdomen sizes comparable to that of Ctrl flies (Supplemental Figure 7B), but smaller heads and brains (Figure 5C-G, and Supplemental Figure 7C, and D). Feeding +WT and +SL larvae with HPA-12 (see Supplemental Methods) restored head size, suggesting that increased *dCERT* activity is responsible for this phenotype (Figure 5F). The levels of Cer and dhCer were significantly and similarly increased in both +WT and +SL strains. Cer-phosphoethanolamine (CPE; the *Drosophila* equivalent of mammalian SM) (51) and dhCPE levels were also increased in both strains, but more substantially in +SL (Figure 5H, and Supplemental Figure 7E-G). These changes are similar to those observed in whole *Drosophila* bodies (Supplemental Figure 7E) and resemble those we observed in mammalian cells (Figure 2B), suggesting that *dCERT* gain of function affects sphingolipid metabolism in flies in a way similar to CerTra mutations in humans. It is

worth noting that glycosphingolipid levels were not significantly altered in +WT and +SL strains, suggesting that changes in Cer, CPE and their dihydro counterparts are sufficient to induce neurological phenotypes in these strains (Supplementary Figure 7E)

As most CerTra patients experience motor delay, we monitored the locomotor activity of the +WT and +SL flies (52). Both +WT and +SL flies showed locomotor hypoactivity compared to Ctrl (Figure 5I). Pre-treatment with HPA-12 (10 μM) for 7 days, which reduced sphingolipid levels (Supplemental Figure 7H), rescued this phenotype in the transgenic lines while having little effect on Ctrl flies (Figure 5J). Moreover, HPA-12 treatment had no effect on the locomotion of a w^{1118} derivative *Drosophila* strain bearing a large chromosomal defect in which the *dCERT* gene is deleted (here referred as KO; Supplemental Figure 7I), suggesting that the HPA-12 effect on locomotion requires *dCERT* expression.

Although the +WT and +SL strains share motor hypoactivity, they do have distinct metabolic phenotypes (Figure 5H), which we hypothesized should produce some difference in phenotype. Because CerTra patients frequently have seizures, we decided to look for seizure-like reactions, such as the paralysis that seizure-susceptible flies often experience after vigorous mechanical stimulation (53, 54). Our strains did not exhibit paralysis upon mechanical stimulation, but the +SL flies showed impaired negative geotaxis that could be corrected by HPA-12 treatment (Figure 5K). Notably, negative geotaxis in non-stressed animals was indistinguishable across genotypes (Supplemental Figure 7J).

These data indicate that an increase in *dCERT* activity in *Drosophila* induces sphingolipid metabolic changes similar to those observed in CerTra syndrome, impairs locomotion, and causes central nervous system vulnerability to mechanical shock in the most severely affected line.

Discussion

In this study we report that multiple *de novo* heterozygous variants in *CERT1* cause an autosomal dominant developmental syndrome we named CerTra, which is characterized by various degrees of developmental delay, motor delay, cognitive impairment, behavioral abnormalities, and seizures. Several CerTra mutations reduce or abolish the capability of CERT to be inactivated in response to excessive sphingomyelin production. This leads to uncontrolled ceramide transfer out of the ER, with several consequences: i) reduced ceramide at the ER relaxes the homeostatic inhibition of serine palmitoyltransferase (55, 56), resulting in increased *de novo* sphingolipid synthesis; ii) reduced ceramide at the Golgi, the site for glucosylceramide synthesis, impairs glycosphingolipid production; and iii) excessive CERT activity likely competes with ceramide desaturase activity at the ER, leading to the transfer of a significant amount of dhCer to the *trans* Golgi and production of dhSM. Elevated dihydro-sphingolipid levels cause neuropathology. For example, biallelic loss-of-function mutations in *DEGS1*, which catalyses the final conversion of dhCer to Cer (Figure 2A), results in increased

dihydro-sphingolipid levels, causing a multisystem neurological disorder of both the central and peripheral nervous system characterised by hypomyelination and leukodystrophy (MIM# 618404) (57, 58). Recessively inherited loss-of-function mutations in alkaline ceramidase 3 (*ACER3*) also result in increased dihydro-sphingolipid formation and a leukodystrophy phenotype (MIM# 617762) (59). Impaired glycosphingolipid synthesis is a further cause of neuropathology: loss-of-function mutations in *ST3GAL5* or *B4GALNT1*, which encode two key enzymes in ganglio-series glycosphingolipid synthesis (i.e., GM3 and GM2 synthases), cause neurodevelopmental regression (MIM# 609056) and spastic paraplegia (MIM# 609195), respectively (60-65). Recently, a specific group of mutations in serine palmitoyltransferase subunits were reported to cause childhood-onset amyotrophic lateral sclerosis (66-68), and hereditary spastic paraplegia (69). All identified mutations disturbed the homeostatic control of *de novo* sphingolipid synthesis, resulting in greatly elevated sphingolipid levels.

Several CerTra mutations cause lipid metabolic derangements similar to those associated with the above listed conditions, nonetheless, the molecular mechanisms of CERT dysregulation appear to be varied. Mutations in the SRR directly impair CERT-inactivating phosphorylation, while mutations in the CCD hinder the conformational change that follows this event. We have not directly addressed the effects of other mutations close to the FFAT motif or in the PH and START domains. These mutations likely affect CERT interaction with VAP proteins (70) and the final events of CERT inactivation that involve intramolecular interactions between the PH and START domains (24). Four consecutive variants (p.R366T, p.I381V, p.E424G, and p.A449V) do not affect CERT localisation nor phosphorylation state. When analysed in greater depth these variants present some doubts about their actual pathogenicity: i) each of them is associated with a single patient and they are not part of a recognisable cluster of mutations; ii) p.I381V has been found in one healthy subject; iii) p.A449V has been found in a subject whose parents (both) presented with intellectual disability independently of the mutational state of *CERT1*; iv) p.R366T has been found in a subject where the very little information we have would point towards a very mild phenotype. Further studies will be required to assess the actual role of these variants and, more in general, to untangle the cellular mechanisms by which sphingolipid metabolism disruption leads to CerTra syndrome. Nonetheless, the characterization of this rare disease entity and of the most frequent variants associated with it has already revealed unforeseen operating principles of sphingolipid homeostasis, led to the definition of a new structural region in CERT, and delineated a possible use of CERT inhibitors for the treatment of CerTra patients.

Methods

Subject identification and clinical characterization

Initial screening and identification of anonymized individuals harbouring *CERT1* variation was conducted through the following public databases and tools: ClinVar (https://www.ncbi.nlm.nih.gov/clinvar/), Decipher (71), GeneMatcher (72), and VKGL-NL Rotterdam (https://www.vkgl.nl/nl/) (Supplemental Table 1). Each patient underwent a full clinical examination by a neurologist and/or medical geneticist. Clinical data were directly abstracted from medical records provided by the referring clinician(s) which included behavioural assessment and electroencephalograms (EEG). Developmental delay and cognitive ability tests were performed on subjects using the following tests: Gesell Developmental Schedules, Chinese National Health Commission Developmental Evaluation Scale, Wechsler Intelligence Scale for Children, Peabody Picture Vocabulary Test-4 (PPVT-4) and Bayley Scales of Infant Development II. When possible, standardised assessment of impairment in conceptual, social, and practical domains in each subject was made in accordance with the Diagnostic and Statistical Manual of Mental Disorders, Fifth Edition (DSM-5) and noted to be mild, moderate, severe or profound. Degrees of intellectual disability (ID) by verbal and nonverbal IQ scores are classified as follows based on verbal and nonverbal IQ scores: mild (IQ 50-55 to ~70), moderate (IQ35-40 to 50-55), severe (IQ 20-25 to 35-40), and profound (IQ <20-25).

To characterise the craniofacial/skeletal dysmorphia, we performed a deep phenotyping analysis for all the patients whose families agreed to share photos. This was done by the team of Eva Bermejo-Sánchez at the Institute of Rare Disease Research (IIER), Madrid (Spain). Dysmorphology analyses were performed blind to the variant detected for each patient. Each parameter was compared to age-, sex-, and ethnicity-matched healthy cases. Briefly, a detailed reading of all the clinical reports was performed to extract a first list of dysmorphic features that was then used to evaluate all the subjects. All the available photographs were assessed based on those features, giving a matrix of 96 rows that were scrutinised for all patients. Thus, the same traits were assessed by the same observer using homogeneous criteria for all the patients. See Supplemental Clinical Appendix for all the features for each patient.

Pathogenicity analysis

All identified variants were analysed in accordance with ACMG Guidelines for variant interpretation and classification (73). Minor allele frequencies (MAF) of all *CERT1* variants were obtained from The Genome Aggregation Database (gnomAD) (74), BRowse All Variants Online (BRAVO) (https://bravo.sph.umich.edu) and the 1,000 Genomes Project (https://www.genome.gov/27528684/1000-genomes-project). Functional annotation of variants was carried out with ANNOtate VARiation (ANNOVAR) (75) using pathogenicity scores of M-CAP (76), REVEL (77), Eigen (78) and CADD (78). As a general guideline, pathogenicity is predicted for variants with scores over 0.025 for M-CAP, 0.5 for REVEL, 0.5 for Eigen and 20 for CADD. Prediction scores of

CerTra variants were compared to other missense variants found in singleton cases amongst the general population in gnomAD (i.e., missense variants reported in only one healthy individual in the gnomAD database).

The analysis of variant clustering was performed as previously described (17, 79). In short, to determine whether the observed variants in patients (17 positions) cluster linearly more than expected compared to random permutations, we calculated the geometric mean distance (δg) between all missense variants on the *CERT1* gene. δg was calculated by taking the mean distance normalised for the transcript length of *CERT1* (hg19:NM_005713.3) over all variant combinations of x_i and x_j of the missense variants, where x represents the position for variant i and j respectively. $1x10^8$ permutations were performed and statistical significance was determined (Fisher's exact test) based on how many times the permuted was smaller or equal to the mean geometric distance observed in our cohort (i.e., significant clustering was determined if the permuted mean distance was larger than observed in our cohort).

Immunofluorescence, staining and image analysis

HeLa cells were grown on glass coverslips, treated according to the experimental procedure, fixed with 4% paraformaldehyde for 15 min at RT and washed three times with PBS. After fixation, cells were blocked with 5% BSA and permeabilized with 0.5% saponin for 20 min at RT, followed by 1 h incubation with selected antibodies against the antigen of interest in blocking solution. Cells were then washed three times with PBS and incubated with appropriate isotype-matched, AlexaFluor-conjugated secondary antibodies diluted in blocking solution for 30 min. After immunostaining, cells were washed three times in PBS and once in water, to remove salts. After Hoechst staining for nuclei, the samples were mounted with Fluoromount-G® (Southern Biotech, 0100-01) on glass microscope slides and analysed under a confocal microscope Leica SP8 with 63x oil objective (1.4 NA), Zeiss LSM700 with 40x oil objective (1.3 NA), or Stellaris-5 with 40x oil objective (1.3 NA). Optical confocal sections were taken at 1 Airy unit under non-saturated conditions with a resolution of 1024x1024 pixels and frame average 2. Images were then processed using Fiji software (https://imagej.net/Fiji) (80).

Statistics

Experimental Design. For protein quantification from patient-derived cell lines, we used values from at least three independent experiments. At every stage of the study, the experimenter was blinded to the identity of control and patient-derived cell lines. For example, Experimenter #1 made a list of samples and controls to be tested, and Experimenter #2 randomised this list and re-labeled the tubes; Experimenter #2 was the only person with the key to identify the samples. These samples were then distributed to

Experimenter #3 to culture the cells, then to Experimenter #1 to perform western blots, and lastly Experimenters #1 and #4 analysed the data. Only then was the key applied to identify the samples.

Software and statistical analysis. Statistical significance ($p<0.05$) was analysed using GraphPad Prism 8 (https://www.graphpad.com/ scientific-software/prism/) and Excel Software (Microsoft). Statistical details and number of replicates for each experiment can be found in the figures and the legends. The range of expression levels in western blots was determined from at least three independent experiments.

Study Approval

All study procedures were defined under protocol #AAAR7750 approved by the Institutional Review Board at Columbia University Irving Medical Center (V.A.G.); the Cambridgeshire Research Ethics Committee for the whole of the UK; the Institutional review board "Commissie MensgebondenOnderzoek Regio Arnhem-Nijmegen under number 2011/188; Hospital Universitario "Virgen de la Arrixaca," Wroclaw Medical University; San Gerardo Hospital, Monza, Italy; Children's Health Ireland at Temple Street Hospital, Dublin, Ireland; the Ethical Committee of the Medical Faculty, Leipzig University (224/16-ek and 402/16-ek); ethics committee of the Instituto de Salud Carlos III.

Full study enrolment (i.e., acquisition of clinical data for further analysis) was conducted only after obtaining written, informed consent/assent for each study subject. The study also adhered to tenets outlined by the Declaration of Helsinki. All patient-related study procedures were conducted according to the respective ethics committees of each participating institution. Specific written, informed consent was also acquired for all subjects whose photographs appear in the manuscript.

Author Contributions

C. Gehin., M.A. Lone, and L. Capolupo designed and performed experiments, analyzed and interpreted the data, and drafted the manuscript; and W. Lee collected all clinical symptoms, analyzed and interpreted clinical data, and drafted the manuscript. S. Ho supported experimental work and contributed to manuscript drafting; S. Zamuner and L.A. Abriata performed structural simulations; V. Kunnathully provided recombinant PKD; B.E. Moeller performed the HDX-MS; J.E. Burke performed and supervised HDX-MS; A. Vocat provided technical support; P. Henklein synthesized synthetic peptides. K. Hanada and T. Yamaji provided *CERT1*-KO cell lines. P. De Los Rios supervised structural simulations. B. Lemaitre, S. Rommelaere, J.-P. Bocquete and E. Ruchti designed the drosophila lines, G. Limoni helped with drosophila locomotor tests under the supervision of B. McCabe. M. Van Campenhoudt designed and constructed the apparatus used for negative geotaxis assay. S. Bourgeat supervised and supported the u-CT experiment under the supervision of A.M. Jaksic. Y. Gupta, T.Y. Lim, and S. Sanna-Cherchi performed the ASD association analysis. E.H. Gerkes provided patient-derived fibroblasts and unaffected

healthy age- sex-matched fibroblasts for Subject 14. E. Lòpez-Martín and E. Bermejo-Sánchez performed craniofacial/skeletal deep phenotyping analysis. E.H. Gerkes, A.P.A. Stegmann, J. Schieving, H. Guo, K. Xia, K. Guo, Q. Zhang, S. Xiong, C.R. Fagerberg, C.P. Bejer, M.J. Larsen, M. Blyth, N. Cooper, V. Wilson, E. Lòpez-Martín, E. Bermejo-Sánchez, B. Martínez-Delgado, R. Oegema, B. Popp, V. Strehlow, D. Gräfe, M. Morleo, A. Seliconi, A. Torella, Y. Herenger, M. Willemsen, F. Soli, A. Murgia, E. Leonardi, R. Śmigiel, C.Gilissen, R. Pfundt, C. Zweier, C. Kraus, V. López-González, L.A. Dulcet, I. Knerr, E. Jones, I. Valenzuela, P. Fernández-Àlvarez. A. Garde, A.L. Bruel, and F. Tran-Mau-Them, G, Costain P. Kannu, A. Adeyemi, A. Marwaha, N.L. Champaigne, M.J. Friez, E.B. Richardson, V.K. Gowda, V.M. Srinivasan, provided clinical data, genetic information, variant re-validation, and comments on the manuscript. A.B.R. Maddocks and J.M. Bain interpreted and analysed the MRIs data. All authors approved the final version of the manuscript.

T. Hornemann, G. D'Angelo, and V.A. Gennarino conceived the study, analysed and interpreted the data, and wrote the manuscript.

Competing Interest

The authors declare no competing interests.

Acknowledgements

We sincerely thank the families who participated in this study and all the staff involved in patient care. We thank Dimitri Moreau and Stefania Vossio (ACCESS Geneva) for microscopy and data analysis; Natalia Gasilova (EPFL ISIC Valais) for native mass spectrometry; the Correia lab at EPFL for support in SEC-MALS; the BIOP, PPSCF and PCF Research Core Facilities at the School of Life Sciences of EPFL, Fani Deverni (FLEXLAB, STI, EPFL) for μ-CT. We also thank M. Chorpra, I. A. Carrera, I. Cusco, B. Molloy (Genuity Science, Ireland Ltd, Dublin/ CHI at Temple Street Rare Disease Research Programme), K. Gorman (CHI at Temple Street, Dublin), M. Posada, J. Alonso, and the entire SpainUDP consortium for help with molecular genetic testing and helpful clinical consultation. We also thank the Undiagnosed Diseases Network International (UDNI) for data sharing. We thank members of the Hornemann, D'Angelo, and Gennarino laboratories for helpful discussions, G. Karsenty for critical comments on the manuscript, and V. Brandt for rigorous editing.

This work was supported by the National Institute of Neurological Disorders and Stroke, NINDS; R01NS109858 (V.A. Gennarino); the Paul A. Marks Scholar Program, Columbia University Vagelos College of Physicians and Surgeons (V.A. Gennarino); the TIGER grant from TAUB Institute, Columbia Vagelos College of Physicians and Scientists (V.A. Gennarino); the Swiss Cancer League, KFS-4999-02-2020 (G. D'Angelo); the EPFL institutional fund (G. D'Angelo); the Kristian Gerhard

Jebsen Foundation (G. D'Angelo); the Swiss National Science Foundation (SNSF) (grant number, 310030_184926, G. D'Angelo); the Natural Science and Engineering Research Council of Canada, Discovery Grant 2020-04241 (J.E. Burke); the Italian Ministry of Health Young Investigator Grant GR-2011-02347754 (E. Leonardi); Fondazione Istituto di Ricerca Pediatrica – Città della Speranza, Grant 18-04 (E. Leonardi); the Wroclaw Medical University grant no. SUB.E160.21.004 (R. Śmigiel); the National Science Centre grant no. OPUS.E160.18.006 (R. Śmigiel); Telethon Undiagnosed Diseases Program (TUDP, GSP15001); Temple Street Foundation/Children's Health Foundation Ireland research grant no. RPAC 19-02 (I. Knerr); The Deutsche Forschungsgemeinschaft (DFG) through grant PO2366/2–1 (B. Popp); The Instituto de Salud Carlos III, Spain (E. López-Martín, E. Bermejo-Sánchez, B. Martínez-Delgado); The National Natural Science Foundation of China, 81871079, 81730036 (H. Guo, and K. Xia); the National Institutes of Diabetes and Digestive and Kidney Diseases, NIDDK; R01 DK115574 (S. Sanna-Cherchi).

This study makes use of data generated by the DEFIDIAG study sponsored by Institute National de la Santé et de la Recherche Médicale (INSERM, France). A full list of centers who contributed to the generation of the data is available from https://defidiag.inserm.fr/ and via email from c16-110.coordo.isp@inserm.fr. The DEFIDIAG study is funded by grants from the French Ministry of Health in the framewok of the national French initiative for genomic medicine. Funding sources were not involved in the study design, data acquisition, analysis, or manuscript writing. This work makes use of Simons Simplex Collection (SSC) data including whole exome sequencing (raw and processed) and associated phenotypic data obtained through SFARI Base (SFARI Request ID : 12030.1.1). This study makes use of data generated by the DECIPHER community. A full list of centers who contributed to the generation of the data is available at https://deciphergenomics.org/about/stats and via email from contact@deciphergenomics.org. Funding for the DECIPHER project was provided by Wellcome. The DDD study presents independent research commissioned by the Health Innovation Challenge Fund [grant number HICF-1009-003], a parallel funding partnership between Wellcome and the Department of Health, and the Wellcome Sanger Institute [grant number WT098051]. The views expressed in this publication are those of the author(s) and not necessarily those of Wellcome or the Department of Health. The study has UK Research Ethics Committee approval (10/H0305/83, granted by the Cambridge South REC, and GEN/284/12 granted by the Republic of Ireland REC). The research team acknowledges the support of the National Institute for Health Research, through the Comprehensive Clinical Research Network.

References

1. Dunn TM, Tifft CJ, and Proia RL. A perilous path: the inborn errors of sphingolipid metabolism. *J Lipid Res.* 2019;60(3):475-83.

2. Hannun YA, and Obeid LM. Sphingolipids and their metabolism in physiology and disease. *Nat Rev Mol Cell Biol.* 2018;19(3):175-91.
3. Ozkara HA. Recent advances in the biochemistry and genetics of sphingolipidoses. *Brain Dev.* 2004;26(8):497-505.
4. Sabourdy F, Astudillo L, Colacios C, Dubot P, Mrad M, Segui B, et al. Monogenic neurological disorders of sphingolipid metabolism. *Biochim Biophys Acta.* 2015;1851(8):1040-51.
5. Breslow DK, and Weissman JS. Membranes in balance: mechanisms of sphingolipid homeostasis. *Mol Cell.* 2010;40(2):267-79.
6. Hanada K, Kumagai K, Yasuda S, Miura Y, Kawano M, Fukasawa M, et al. Molecular machinery for non-vesicular trafficking of ceramide. *Nature.* 2003;426(6968):803-9.
7. Fugmann T, Hausser A, Schöffler P, Schmid S, Pfizenmaier K, and Olayioye MA. Regulation of secretory transport by protein kinase D-mediated phosphorylation of the ceramide transfer protein. *J Cell Biol.* 2007;178(1):15-22.
8. de Ligt J, Willemsen MH, van Bon BWM, Kleefstra T, Yntema HG, Kroes T, et al. Diagnostic exome sequencing in persons with severe intellectual disability. *N Engl J Med.* 2012;367(20):1921-9.
9. De Rubeis S, He X, Goldberg AP, Poultney CS, Samocha K, Cicek AE, et al. Synaptic, transcriptional and chromatin genes disrupted in autism. *Nature.* 2014;515(7526):209-15.
10. Hamdan FF, Srour M, Capo-Chichi J-M, Daoud H, Nassif C, Patry L, et al. De novo mutations in moderate or severe intellectual disability. *PLoS Genet.* 2014;10(10):e1004772.
11. Helbig KL, Farwell Hagman KD, Shinde DN, Mroske C, Powis Z, Li S, et al. Diagnostic exome sequencing provides a molecular diagnosis for a significant proportion of patients with epilepsy. *Genet Med.* 2016;18(9):898-905.
12. Iossifov I, O'Roak BJ, Sanders SJ, Ronemus M, Krumm N, Levy D, et al. The contribution of de novo coding mutations to autism spectrum disorder. *Nature.* 2014;515(7526):216-21.
13. Murakami H, Tamura N, Enomoto Y, Shimasaki K, Kurosawa K, and Hanada K. Intellectual disability-associated gain-of-function mutations in CERT1 that encodes the ceramide transport protein CERT. *PLoS One.* 2020;15(12):e0243980.
14. Study TDDD, and The Deciphering Developmental Disorders S. Large-scale discovery of novel genetic causes of developmental disorders. *Nature.* 2015;519(7542):223-8.
15. Takata A, Miyake N, Tsurusaki Y, Fukai R, Miyatake S, Koshimizu E, et al. Integrative Analyses of De Novo Mutations Provide Deeper Biological Insights into Autism Spectrum Disorder. *Cell Rep.* 2018;22(3):734-47.
16. Wang T, Guo H, Xiong B, Stessman HA, Wu H, Coe BP, et al. De novo genic mutations among a Chinese autism spectrum disorder cohort. *Nat Commun.* 2016;7:13316.
17. Lee W, de Prisco N, and Gennarino VA. Identifying patients and assessing variant pathogenicity for an autosomal dominant disease-driving gene. *STAR Protoc.* 2022;3(1):101150.
18. Edition F, and Others. Diagnostic and statistical manual of mental disorders. *Am Psychiatric Assoc.* 2013;21.
19. Satterstrom FK, Kosmicki JA, Wang J, Breen MS, De Rubeis S, An JY, et al. Large-Scale Exome Sequencing Study Implicates Both Developmental and Functional Changes in the Neurobiology of Autism. *Cell.* 2020;180(3):568-84 e23.
20. Prashek J, Bouyain S, Fu M, Li Y, Berkes D, and Yao X. Interaction between the PH and START domains of ceramide transfer protein competes with phosphatidylinositol 4-phosphate binding by the PH domain. *J Biol Chem.* 2017;292(34):14217-28.
21. Baron CL, and Malhotra V. Role of diacylglycerol in PKD recruitment to the TGN and protein transport to the plasma membrane. *Science.* 2002;295(5553):325-8.
22. Capasso S, Sticco L, Rizzo R, Pirozzi M, Russo D, Dathan NA, et al. Sphingolipid metabolic flow controls phosphoinositide turnover at the trans-Golgi network. *EMBO J.* 2017;36(12):1736-54.

23. Luberto C, and Hannun YA. Sphingomyelin synthase, a potential regulator of intracellular levels of ceramide and diacylglycerol during SV40 transformation: does sphingomyelin synthase account for the putative phosphatidylcholine-specific phospholipase C? *J Biol Chem.* 1998;273(23):14550-9.
24. Kumagai K, Kawano M, Shinkai-Ouchi F, Nishijima M, and Hanada K. Interorganelle Trafficking of Ceramide Is Regulated by Phosphorylation-dependent Cooperativity between the PH and START Domains of CERT*. *J Biol Chem.* 2007;282(24):17758-66.
25. Prashek J, Truong T, and Yao X. Crystal structure of the pleckstrin homology domain from the ceramide transfer protein: implications for conformational change upon ligand binding. *PLoS One.* 2013;8(11):e79590.
26. Sugiki T, Egawa D, Kumagai K, Kojima C, Fujiwara T, Takeuchi K, et al. Phosphoinositide binding by the PH domain in ceramide transfer protein (CERT) is inhibited by hyperphosphorylation of an adjacent serine-repeat motif. *J Biol Chem.* 2018;293(28):11206-17.
27. Tomishige N, Kumagai K, Kusuda J, Nishijima M, and Hanada K. Casein kinase I{gamma}2 down-regulates trafficking of ceramide in the synthesis of sphingomyelin. *Mol Biol Cell.* 2009;20(1):348-57.
28. Thomaseth C, Weber P, Hamm T, Kashima K, and Radde N. Modeling sphingomyelin synthase 1 driven reaction at the Golgi apparatus can explain data by inclusion of a positive feedback mechanism. *J Theor Biol.* 2013;337:174-80.
29. Saito S, Matsui H, Kawano M, Kumagai K, Tomishige N, Hanada K, et al. Protein Phosphatase 2Cϵ Is an Endoplasmic Reticulum Integral Membrane Protein That Dephosphorylates the Ceramide Transport Protein CERT to Enhance Its Association with Organelle Membranes*. *J Biol Chem.* 2008;283(10):6584-93.
30. Tamura N, Sakai S, Martorell L, Colome R, Mizuike A, Goto A, et al. Intellectual-disability-associated mutations in the ceramide transport protein gene CERT1 lead to aberrant function and subcellular distribution. *J Biol Chem.* 2021;297(5):101338.
31. Goto A, Egawa D, Tomishige N, Yamaji T, Shimasaki K, Kumagai K, et al. Involvement of a Cluster of Basic Amino Acids in Phosphorylation-Dependent Functional Repression of the Ceramide Transport Protein CERT. *Int J Mol Sci.* 2022;23(15).
32. Lone MA, Hülsmeier AJ, Saied EM, Karsai G, Arenz C, von Eckardstein A, et al. Subunit composition of the mammalian serine-palmitoyltransferase defines the spectrum of straight and methyl-branched long-chain bases. *Proc Natl Acad Sci U S A.* 2020;117(27):15591-8.
33. Ternes P, Franke S, Zähringer U, Sperling P, and Heinz E. Identification and characterization of a sphingolipid delta 4-desaturase family. *J Biol Chem.* 2002;277(28):25512-8.
34. Wang Y, Niu Y, Zhang Z, Gable K, Gupta SD, Somashekarappa N, et al. Structural insights into the regulation of human serine palmitoyltransferase complexes. *Nat Struct Mol Biol.* 2021;28(3):240-8.
35. Yamaji T, and Hanada K. Establishment of HeLa cell mutants deficient in sphingolipid-related genes using TALENs. *PLoS One.* 2014;9(2):e88124.
36. Davis DL, Gable K, Suemitsu J, Dunn TM, and Wattenberg BW. The ORMDL/Orm–serine palmitoyltransferase (SPT) complex is directly regulated by ceramide: Reconstitution of SPT regulation in isolated membranes. *J Biol Chem.* 2019;294(13):5146-56.
37. Yasuda S, Kitagawa H, Ueno M, Ishitani H, Fukasawa M, Nishijima M, et al. A Novel Inhibitor of Ceramide Trafficking from the Endoplasmic Reticulum to the Site of Sphingomyelin Synthesis*. *J Biol Chem.* 2001;276(47):43994-4002.
38. Kudo N, Kumagai K, Tomishige N, Yamaji T, Wakatsuki S, Nishijima M, et al. Structural basis for specific lipid recognition by CERT responsible for nonvesicular trafficking of ceramide. *Proc Natl Acad Sci U S A.* 2008;105(2):488-93.
39. Sugiki T, Takeuchi K, Yamaji T, Takano T, Tokunaga Y, Kumagai K, et al. Structural basis for the Golgi association by the pleckstrin homology domain of the ceramide trafficking protein (CERT). *J Biol Chem.* 2012;287(40):33706-18.

40. Charruyer A, Bell SM, Kawano M, Douangpanya S, Yen T-Y, Macher BA, et al. Decreased Ceramide Transport Protein (CERT) Function Alters Sphingomyelin Production following UVB Irradiation*. *J Biol Chem.* 2008;283(24):16682-92.
41. UniProt C. UniProt: a worldwide hub of protein knowledge. *Nucleic Acids Res.* 2019;47(D1):D506-D15.
42. Engen JR, Botzanowski T, Peterle D, Georgescauld F, and Wales TE. Developments in Hydrogen/Deuterium Exchange Mass Spectrometry. *Anal Chem.* 2021;93(1):567-82.
43. Masson GR, Burke JE, Ahn NG, Anand GS, Borchers C, Brier S, et al. Recommendations for performing, interpreting and reporting hydrogen deuterium exchange mass spectrometry (HDX-MS) experiments. *Nat Methods.* 2019;16(7):595-602.
44. Yang J, Anishchenko I, Park H, Peng Z, Ovchinnikov S, and Baker D. Improved protein structure prediction using predicted interresidue orientations. *Proc Natl Acad Sci U S A.* 2020;117(3):1496-503.
45. Jumper J, Evans R, Pritzel A, Green T, Figurnov M, Ronneberger O, et al. Highly accurate protein structure prediction with AlphaFold. *Nature.* 2021;596(7873):583-9.
46. Trigg J, Gutwin K, Keating AE, and Berger B. Multicoil2: predicting coiled coils and their oligomerization states from sequence in the twilight zone. *PLoS One.* 2011;6(8):e23519.
47. van den Heuvel RHH, and Heck AJR. Native protein mass spectrometry: from intact oligomers to functional machineries. *Curr Opin Chem Biol.* 2004;8(5):519-26.
48. Mogridge J. In: Meyerkord CL, and Fu H eds. *Protein-Protein Interactions: Methods and Applications*. New York, NY: Springer New York; 2015:233-8.
49. Revert F, Revert-Ros F, Blasco R, Artigot A, Lopez-Pascual E, Gozalbo-Rovira R, et al. Selective targeting of collagen IV in the cancer cell microenvironment reduces tumor burden. *Oncotarget.* 2018;9(13):11020-45.
50. Rao RP, Yuan C, Allegood JC, Rawat SS, Edwards MB, Wang X, et al. Ceramide transfer protein function is essential for normal oxidative stress response and lifespan. *Proc Natl Acad Sci U S A.* 2007;104(27):11364-9.
51. Rietveld A, Neutz S, Simons K, and Eaton S. Association of sterol- and glycosylphosphatidylinositol-linked proteins with Drosophila raft lipid microdomains. *J Biol Chem.* 1999;274(17):12049-54.
52. Pfeiffenberger C, Lear BC, Keegan KP, and Allada R. Locomotor activity level monitoring using the Drosophila Activity Monitoring (DAM) System. *Cold Spring Harb Protoc.* 2010;2010(11):pdb prot5518.
53. Benzer S. From the gene to behavior. *JAMA.* 1971;218(7):1015-22.
54. Pavlidis P, Ramaswami M, and Tanouye MA. The Drosophila easily shocked gene: a mutation in a phospholipid synthetic pathway causes seizure, neuronal failure, and paralysis. *Cell.* 1994;79(1):23-33.
55. Breslow DK, Collins SR, Bodenmiller B, Aebersold R, Simons K, Shevchenko A, et al. Orm family proteins mediate sphingolipid homeostasis. *Nature.* 2010;463(7284):1048-53.
56. Clarke BA, Majumder S, Zhu H, Lee YT, Kono M, Li C, et al. The Ormdl genes regulate the sphingolipid synthesis pathway to ensure proper myelination and neurologic function in mice. *Elife.* 2019;8.
57. Karsai G, Kraft F, Haag N, Korenke GC, Hänisch B, Othman A, et al. DEGS1-associated aberrant sphingolipid metabolism impairs nervous system function in humans. *J Clin Invest.* 2019;129(3):1229-39.
58. Pant DC, Aguilera-Albesa S, and Pujol A. Ceramide signalling in inherited and multifactorial brain metabolic diseases. *Neurobiol Dis.* 2020;143:105014.
59. Edvardson S, Yi JK, Jalas C, Xu R, Webb BD, Snider J, et al. Deficiency of the alkaline ceramidase ACER3 manifests in early childhood by progressive leukodystrophy. *J Med Genet.* 2016;53(6):389-96.

60. Bhuiyan RH, Ohmi Y, Ohkawa Y, Zhang P, Takano M, Hashimoto N, et al. Loss of Enzyme Activity in Mutated B4GALNT1 Gene Products in Patients with Hereditary Spastic Paraplegia Results in Relatively Mild Neurological Disorders: Similarity with Phenotypes of B4galnt1 Knockout Mice. *Neuroscience.* 2019;397:94-106.
61. Boccuto L, Aoki K, Flanagan-Steet H, Chen CF, Fan X, Bartel F, et al. A mutation in a ganglioside biosynthetic enzyme, ST3GAL5, results in salt & pepper syndrome, a neurocutaneous disorder with altered glycolipid and glycoprotein glycosylation. *Hum Mol Genet.* 2014;23(2):418-33.
62. Harlalka GV, Lehman A, Chioza B, Baple EL, Maroofian R, Cross H, et al. Mutations in B4GALNT1 (GM2 synthase) underlie a new disorder of ganglioside biosynthesis. *Brain.* 2013;136(Pt 12):3618-24.
63. Simpson EP, Henry YK, Henkel JS, Smith RG, and Appel SH. Increased lipid peroxidation in sera of ALS patients: a potential biomarker of disease burden. *Neurology.* 2004;62(10):1758-65.
64. Wakil SM, Monies DM, Ramzan K, Hagos S, Bastaki L, Meyer BF, et al. Novel B4GALNT1 mutations in a complicated form of hereditary spastic paraplegia. *Clin Genet.* 2014;86(5):500-1.
65. Wang H, Wang A, Wang D, Bright A, Sency V, Zhou A, et al. Early growth and development impairments in patients with ganglioside GM3 synthase deficiency. *Clin Genet.* 2016;89(5):625-9.
66. Grob JJ, Collet-Villette AM, and Bonerandi JJ. [Piezogenic cellulo-adipose hernia of the leg]. *Ann Dermatol Venereol.* 1987;114(12):1567-9.
67. Lone MA, Aaltonen MJ, Zidell A, Pedro HF, Morales Saute JA, Mathew S, et al. SPTLC1 variants associated with ALS produce distinct sphingolipid signatures through impaired interaction with ORMDL proteins. *J Clin Invest.* 2022;132(18).
68. Mohassel P, Donkervoort S, Lone MA, Nalls M, Gable K, Gupta SD, et al. Childhood amyotrophic lateral sclerosis caused by excess sphingolipid synthesis. *Nat Med.* 2021.
69. Srivastava S, Shaked HM, Gable K, Gupta SD, Pan X, Somashekarappa N, et al. SPTSSA variants alter sphingolipid synthesis and cause a complex hereditary spastic paraplegia. *Brain.* 2023.
70. Kawano M, Kumagai K, Nishijima M, and Hanada K. Efficient Trafficking of Ceramide from the Endoplasmic Reticulum to the Golgi Apparatus Requires a VAMP-associated Protein-interacting FFAT Motif of CERT*. *J Biol Chem.* 2006;281(40):30279-88.
71. Firth HV, Richards SM, Bevan AP, Clayton S, Corpas M, Rajan D, et al. DECIPHER: Database of Chromosomal Imbalance and Phenotype in Humans Using Ensembl Resources. *Am J Hum Genet.* 2009;84(4):524-33.
72. Sobreira N, Schiettecatte F, Valle D, and Hamosh A. GeneMatcher: a matching tool for connecting investigators with an interest in the same gene. *Hum Mutat.* 2015;36(10):928-30.
73. Richards S, on behalf of the ALQAC, Aziz N, Bale S, Bick D, Das S, et al. Standards and guidelines for the interpretation of sequence variants: a joint consensus recommendation of the American College of Medical Genetics and Genomics and the Association for Molecular Pathology. *Genetics in Medicine.* 2015;17(5):405-23.
74. Karczewski KJ, Francioli LC, Tiao G, Cummings BB, Alfoldi J, Wang Q, et al. The mutational constraint spectrum quantified from variation in 141,456 humans. *Nature.* 2020;581(7809):434-43.
75. Wang K, Li M, and Hakonarson H. ANNOVAR: functional annotation of genetic variants from high-throughput sequencing data. *Nucleic Acids Res.* 2010;38(16):e164.
76. Jagadeesh KA, Wenger AM, Berger MJ, Guturu H, Stenson PD, Cooper DN, et al. M-CAP eliminates a majority of variants of uncertain significance in clinical exomes at high sensitivity. *Nat Genet.* 2016;48(12):1581-6.
77. Ioannidis NM, Rothstein JH, Pejaver V, Middha S, McDonnell SK, Baheti S, et al. REVEL: An Ensemble Method for Predicting the Pathogenicity of Rare Missense Variants. *Am J Hum Genet.* 2016;99(4):877-85.

78. Ionita-Laza I, McCallum K, Xu B, and Buxbaum JD. A spectral approach integrating functional genomic annotations for coding and noncoding variants. *Nat Genet.* 2016;48(2):214-20.
79. Lelieveld SH, Wiel L, Venselaar H, Pfundt R, Vriend G, Veltman JA, et al. Spatial Clustering of de Novo Missense Mutations Identifies Candidate Neurodevelopmental Disorder-Associated Genes. *Am J Hum Genet.* 2017;101(3):478-84.
80. Schindelin J, Arganda-Carreras I, Frise E, Kaynig V, Longair M, Pietzsch T, et al. Fiji: an open-source platform for biological-image analysis. *Nat Methods.* 2012;9(7):676-82.

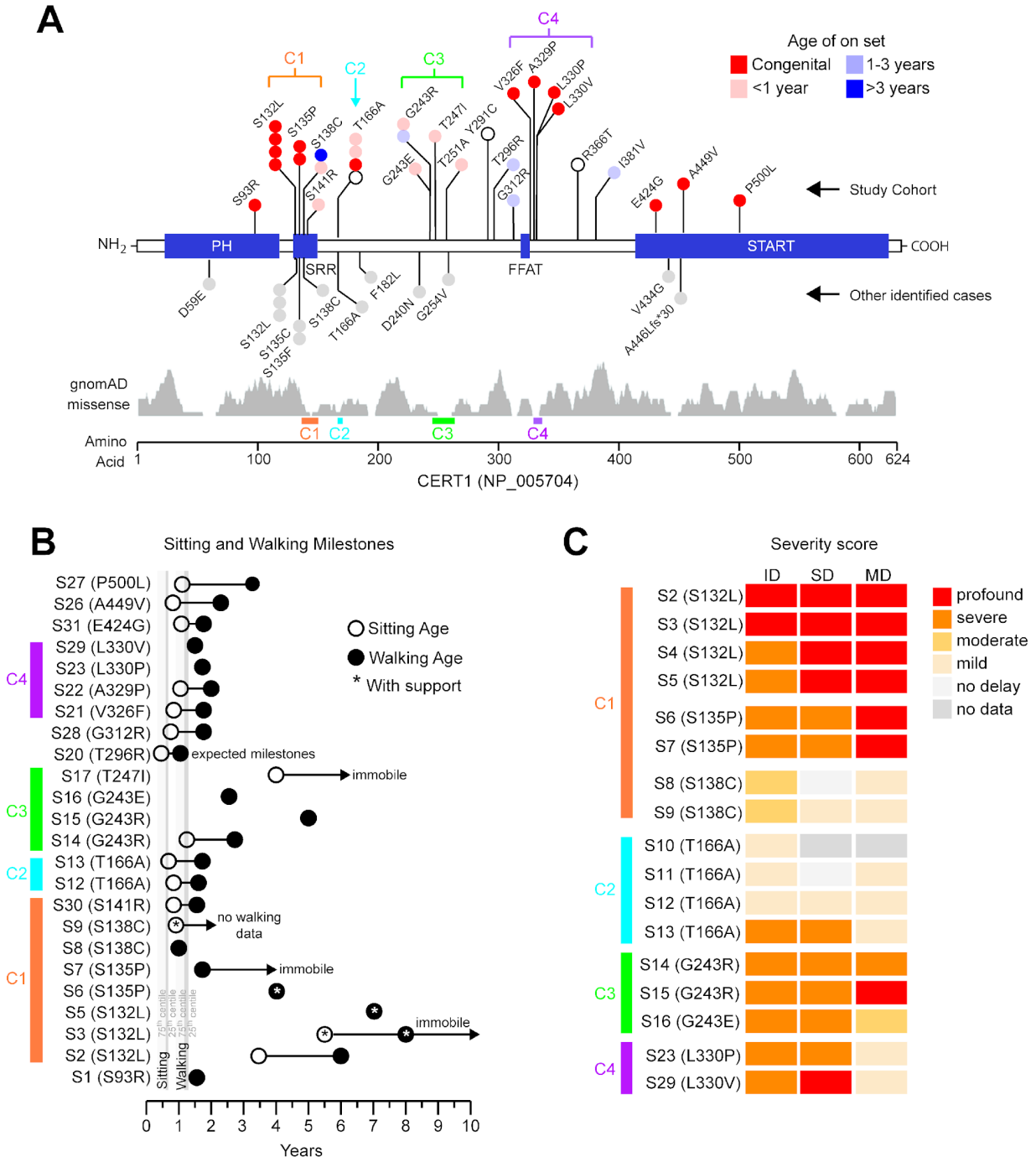

Figure 1. Mutations in *CERT1* lead to a neurodevelopmental syndrome. (A) Schematic representation

of functional domains in CERT. The N-terminal Pleckstrin Homology (PH) domain interacts with phosphoinositide phosphatidylinositol-4-phosphate [PtdIns(4)*P*] (20) on the *trans* Golgi. The serine rich region (SRR) is the target of protein kinase D (PKD) and casein kinase 1γ2 (CSNK1G2) phosphorylation. The FFAT (two phenylalanines in an acidic tract) motif interacts with integral membrane proteins VAP-A and VAP-B on the ER (70), and a C-terminal (StAR)-related lipid transfer (START) domain extracts ceramide from the ER membrane and delivers it to the *trans* Golgi (6). The schematic shows coding variants in *CERT1* (NP_005704) in our cohort of 31 subjects above the gene diagram and other individuals identified from clinical databases (Decipher v9. 31, ClinVar and VKGL) below it (Supplemental Table 1). Colors indicate the age of onset; grey, no information available. The distribution of gnomAD singleton missense variants for healthy subjects is plotted below. **(B)** Range of severity in motor delays compared to the 75th percentile (light grey) and 25th percentile (dark grey), adapted from values published by the Denver Developmental Screening Test II. Open and closed circles indicate delayed sitting and walking ages, respectively; asterisks indicate the subject needs sitting or walking support. Open arrows indicate subjects who are currently immobile or have not yet developed independent walking. Clusters mutations belong to are indicated. **(C)** Heatmap displaying the degree of intellectual disability (ID), speech delay (SD), and motor delay (MD) of patients bearing frequent *CERT1* mutations. See Supplemental Table 2 for scores.

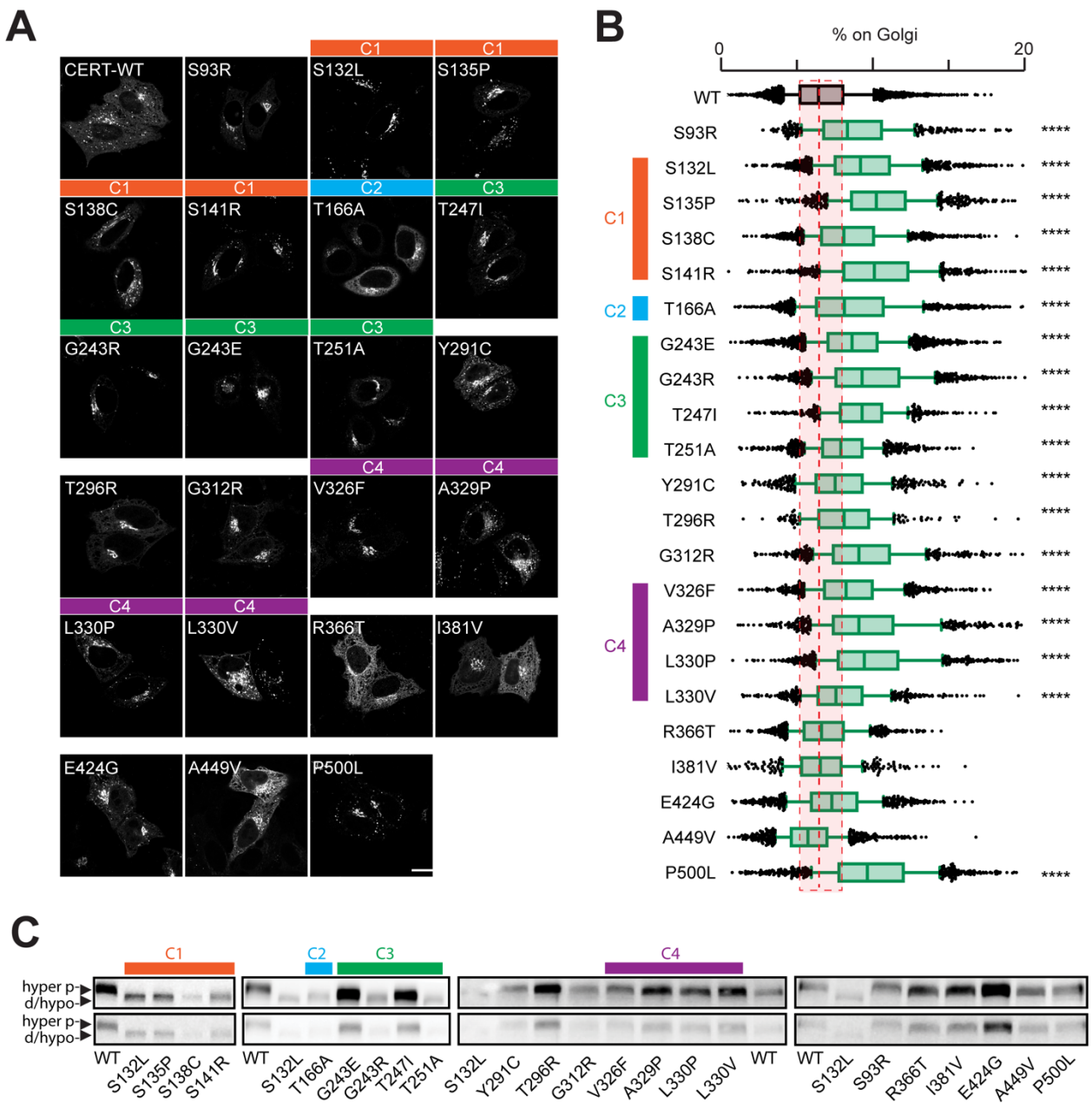

Figure 2. Disease-causing variants cause CERT mis-regulation. (A) CERT-GFP WT and mutant localization in HeLa cells analysed by confocal microscopy. Scale bar, 20 µm. Clusters as in Figure 1 are indicated throughout. **(B)** Percentage of CERT-GFP WT and mutants associated with the Golgi complex in HeLa cells. Cells were stained with Hoechst and anti-GM130 antibody and analysed by automated fluorescence microscopy (n>1,000 cells per condition; ****p <0.0001 [one-way ANOVA], effect size >15%). CERT WT in grey, CerTra mutants in green). Data are shown as box-and-whisker plots. Bars represent the median value of each dataset. Clusters mutations belong to are indicated. **(C)** Western blot of HeLa cells expressing CERT-GFP WT or mutants (n=3). Hyperphosphorylated (hyper p-) and de/hypophosphorylated (d/hypo-) bands are indicated by arrowheads.

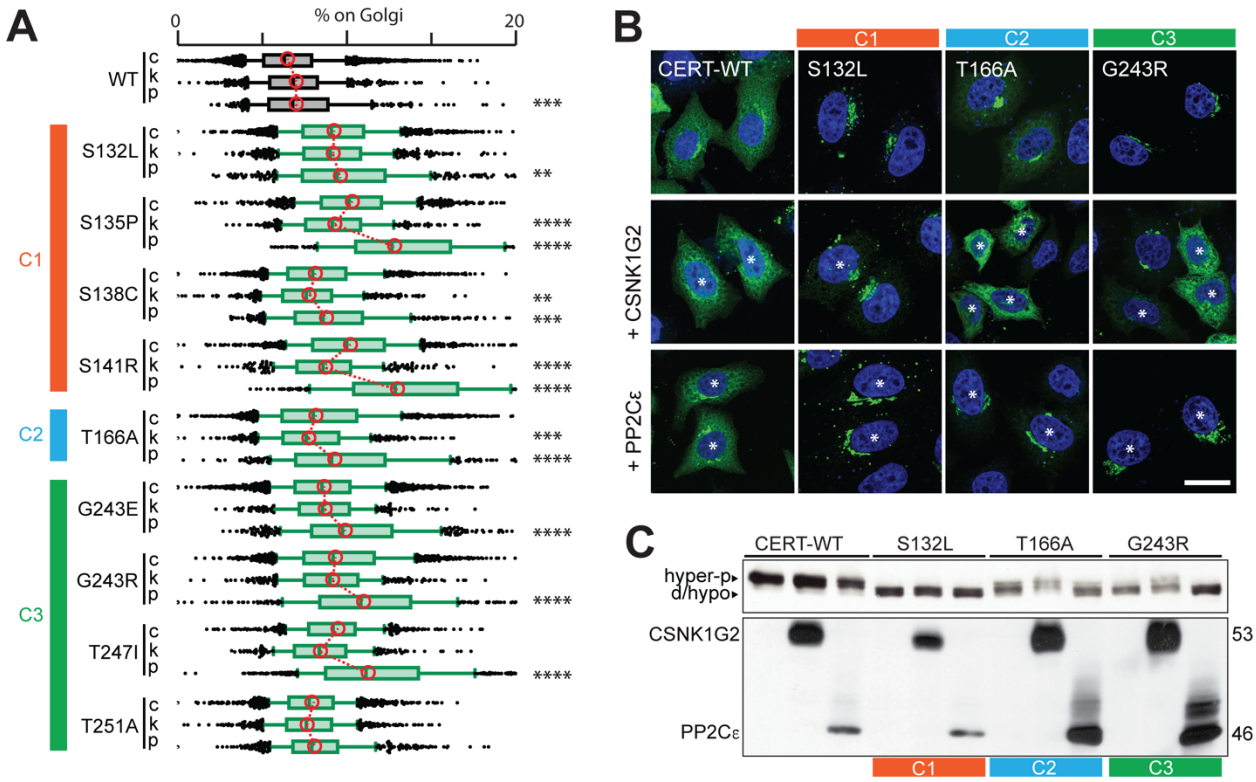

Figure 3. Disease-causing CERT variants are susceptible to phospho-regulation. (A) Percentage of CERT-GFP WT and mutants from Clusters 1, 2 and 3 associated with the Golgi complex in HeLa cells overexpressing CSNK1G2-HA (k) or PP2Cε-HA (p). Cells were stained with Hoechst, anti-GM130 and anti-HA antibodies and analysed by automated fluorescence microscopy (n>500 cells per condition; **p <0.01, ***p <0.001, ****p<0.0001 [one-way ANOVA]). Bars represent the median value of each dataset. **(B)** Subcellular localization of CERT-GFP WT, p.S132L, p.T166A, p.G243R in HeLa cells expressing PP2Cε-HA or CSNK1G-HA. Cells were stained with DAPI (blue) and anti-HA antibody and analysed by confocal microscopy. Asterisks indicate co-transfected cells. Scale bar, 20 µm. **(C)** Western blot analysis of HeLa cells co-expressing CERT-GFP WT or mutants with CSNK1G2-HA or PP2Cε-HA (n=3).

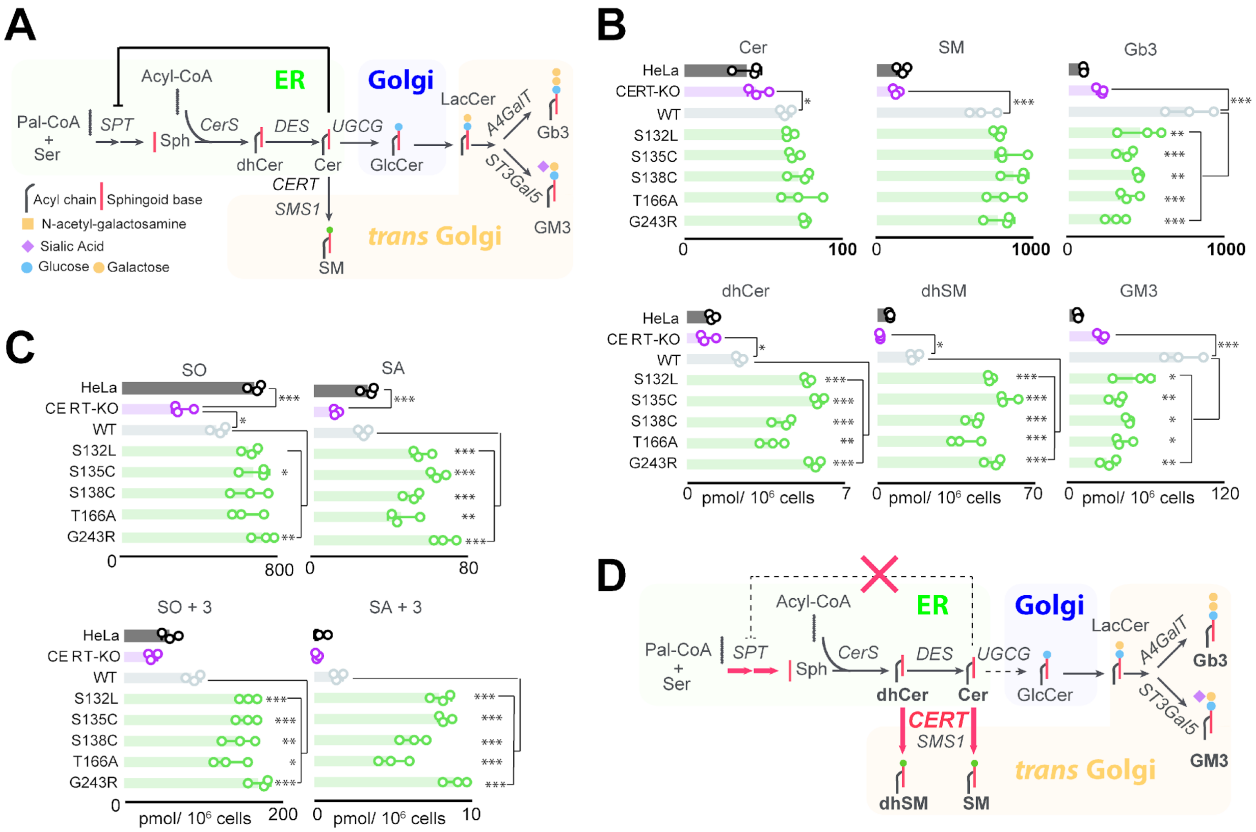

Figure 4. Several *CERT1* mutations increase sphingolipid levels. (A) Schematic representation of the *de novo* sphingolipid biosynthetic pathway with the main enzymes involved (Shading indicates the prevalent intracellular localisation of synthetic reactions). SPT, serine palmitoyltransferase; CerS, ceramide synthases; DES, dihydro-ceramide desaturase; SMS1, sphingomyelin synthase 1; UGCG, glucosylceramide synthase; ST3Gal5, GM3 synthase; A4GalT, Gb3 synthase. **(B)** Mass spectrometry profile of sphingolipids in HeLa *CERT1*-KO cells overexpressing selected *CERT1* mutants from Clusters 1, 2, and 3. Values are total levels across the major fatty acid chain lengths of indicated sphingolipids, the levels of individual species are reported in Supplemental Figure 4A. (n=3; data are means ± SD; *p <0.05, **p <0.01, ***p <0.001 [one-way ANOVA]). **(C)** Effect of CERT mutations in HeLa cells on the long chain bases (LCB). LCB profiles were evaluated by incorporation of isotope labelled (2,3,3-D^3, ^{15}N)-L-serine. SO, sphingosine; SA, sphinganine. (n=3; data are means ± SD; *p <0.05, **p <0.01, ***p <0.001 [one-way ANOVA]). **(D)** The *de novo* sphingolipid biosynthetic pathway as modified by *CERT1* mutations in Clusters 1, 2, and 3.

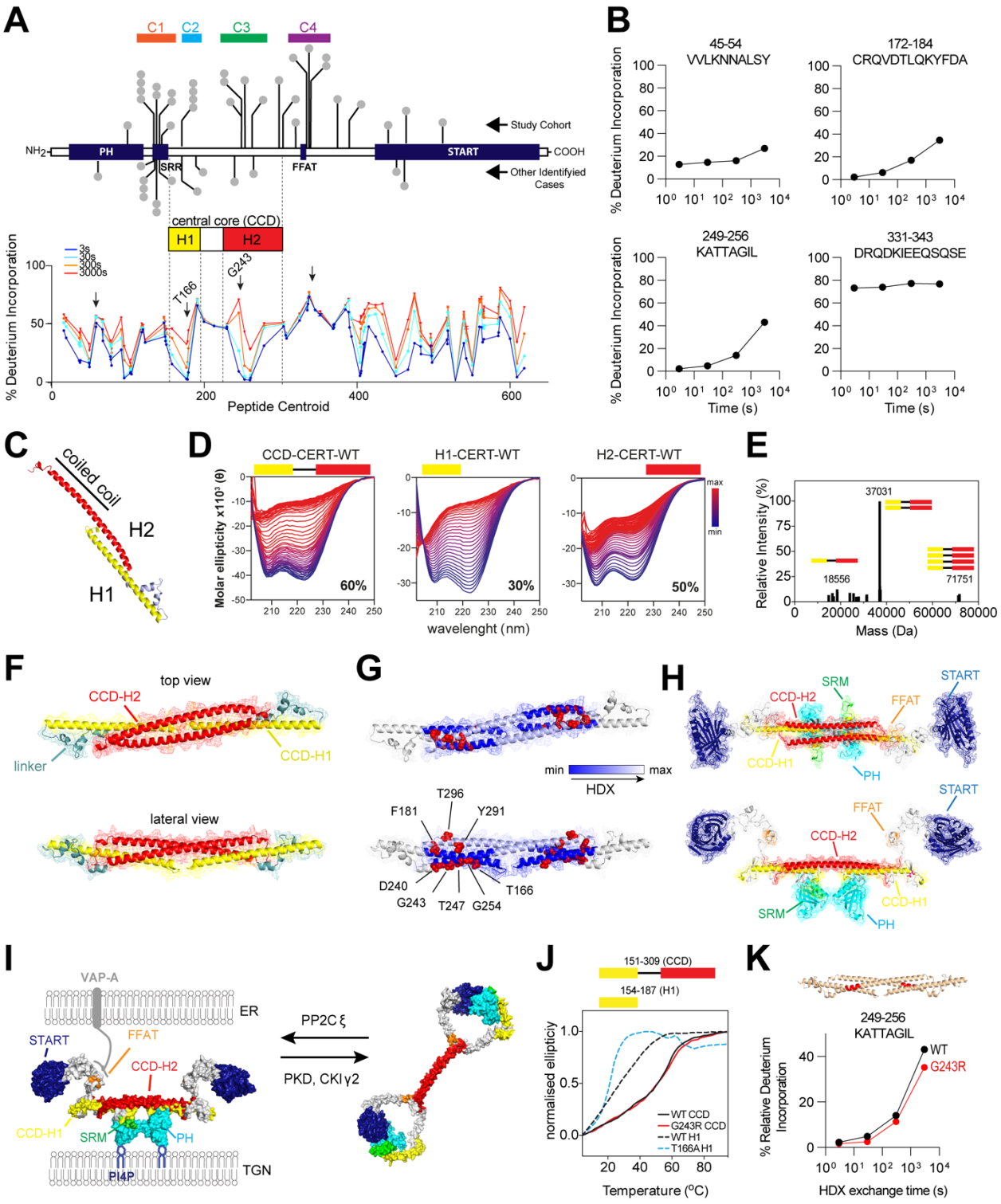

Figure 5. Disease-causing *CERT1* mutations affect the central core structure of CERT. (A) Domain organisation of CERT with its central core domain (CCD) and the predicted H1 and H2 helices. Global percentage of HDX (hydrogen deuterium exchange) shown for all peptides graphed according to their central residue number. The mean of three experiments is shown. **(B)** Deuterium incorporation over time of four selected peptides (Highlighted with arrows on the HDX profile). Data are from Supplemental

Tables 5 and 6. **(C)** Molecular model of CERT's central core domain (CCD) based on contact prediction. Helix H1 is denoted yellow and H2 as red. **(D)** Thermostability of intervening regions showing a difference in HDX by circular dichroism: the samples were heated from 4°C to 94°C; the percentage indicates the helicity of each construct at 20°C. **(E)** Deconvoluted mass spectrum of purified recombinant CERT 151-309 WT. 18.5kDa represents the molecular weight of the monomer, 37 kDa, a dimer and 71.5 kDa a tetramer. **(F)** Molecular model of CERT 151-309 WT as an antiparallel dimer. **(G)** Model showing the location of amino acids mutated in CerTra syndrome. The areas differentially exposed to deuterium exchange are indicated according to the colour scale. **(H)** Molecular model of CERT WT as an antiparallel dimer. **(I)** Molecular model of CERT WT at the ER-TGN membrane contact site in its active and inactive conformations. **(J)** Thermostability of CERT 154-187 WT and p.T166A, CERT 151-309 WT and p.G243R by circular dichroism. **(K)** Peptide in the CCD displaying decreases in exchange in p.G243R mutant compared to WT. These changes are mapped on the hypothetical CCD structure.

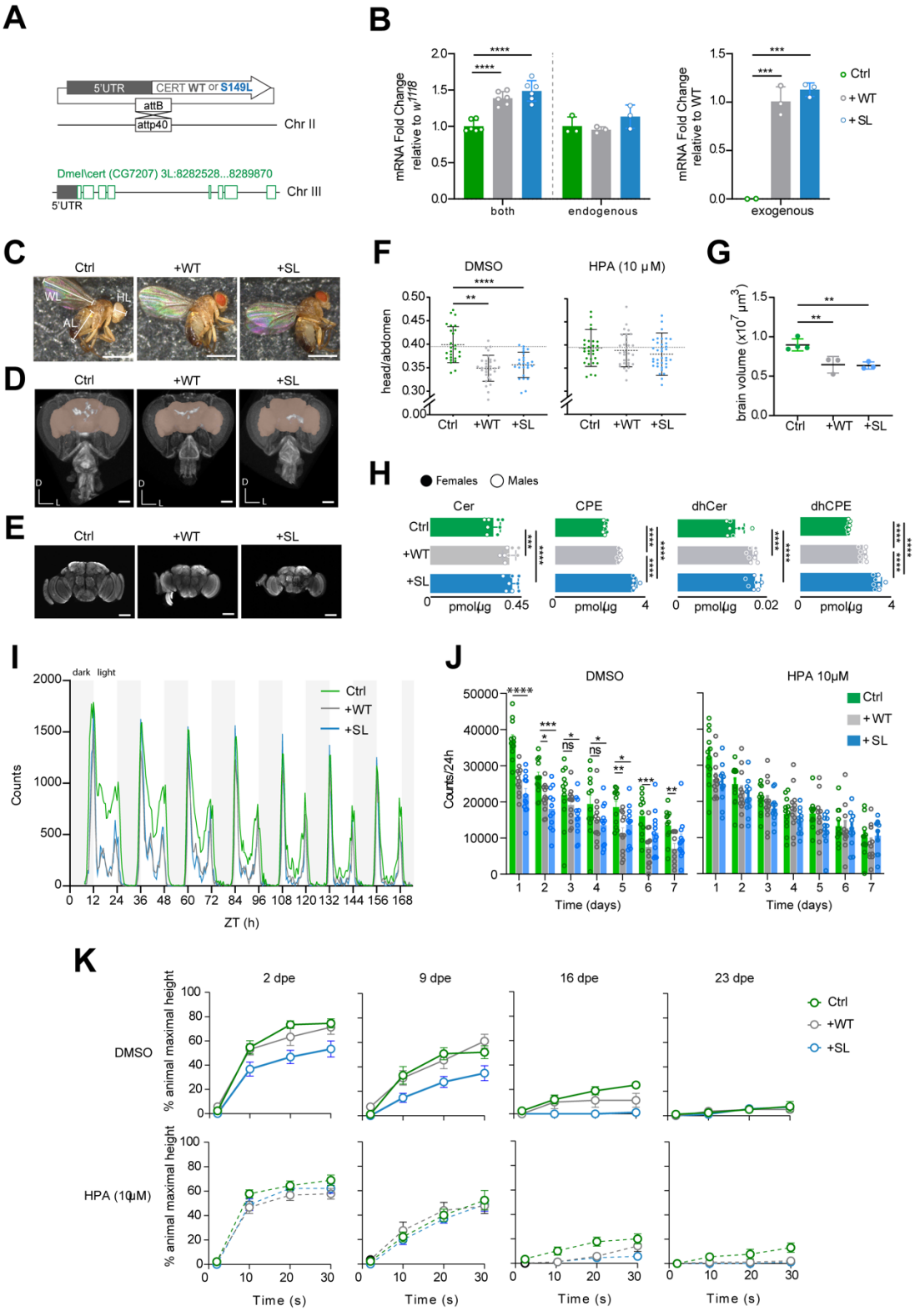

Figure 6. CERT gain of function causes neurological defects in *Drosophila melanogaster.* (A) Schematic of transgenic *dCERT* flies in the w^{1118} background. $dCERT^{WT}$, +WT; $dCERT^{p.S149L}$, +SL. **(B)** Quantification of endogenous or exogenous *dCERT* mRNA levels in w^{1118} background (Ctrl) or *dCERT*

transgenic flies. Data shown are $\log_2$ fold change over Ctrl or +WT (n=6; data are mean ± SD). Here and throughout this figure, the statistics were calculated by one-way ANOVA, with asterisks as follows: *p <0.05, **p <0.01, ***p <0.001, ****p<0.0001. [one-way ANOVA]). **(C)** Representative specimens of Ctrl, +WT and +SL adult flies. Head length (HL), abdomen length (AL) and wing length (WL) were measured. Scale bar, 1 mm. **(D)** 3D rendering of µ-CT scan of the heads from Ctrl, +WT and +SL adults (frontal view). Brain volume is highlighted in pink. Body axes are Dorsal (D) and Left (L). Scale bar, 100 µm. **(E)** Z-projections of confocal stacks of whole-mount adult Ctrl, +WT and +SL adult brains (frontal view) immunostained with anti-nc82. Scale bar, 100 µm. **(F**) Head/abdomen length ratio (HL/AL) of flies reared on DMSO or 10 µM HPA-12 (Ctrl n=26 or 30*,* +WT n=31 or 31 and +SL n=25 or 38). **(G)** Brain volume from Ctrl, +WT and +SL flies acquired by confocal microscopy (n=3-4; data are means ± SEM). **(H)** Mass spectrometry profile of sphingolipids in Ctrl, +WT and +SL adult heads. Cer, ceramide; dhCer, dihydro-ceramide; CPE, ceramide phosphoethanolamine; dhCPE, dihydro-ceramide phosphoethanolamine (n = 8). **(I)** Locomotion of Ctrl, +WT and +SL flies plotted as total counts per 30 min over time (n = 16). **(J)** Locomotion of flies pre-treated with 0 or 10 µM HPA-12 (n = 12). **(K)** Climbing ability of flies at dpe 2, 9, 16 and 23 after vigorous mechanical stress (n = 9). Data shown is mean ± SEM.

Table 1. Phenotype-genotype correlations for variants for which we have more than one subject. Although it is difficult to draw firm conclusions from two to four patients, we can sketch the main features that are associated with each variant thus far, based on available information. Please see the Clinical Appendix and Supplemental Table 2 for details on all 31 subjects.

Variant	Key features
S132L (n=4, S2-S5)	Small at birth, perinatal difficulties, failure to thrive. Achieve sitting at 3-4 years; may walk, supported, by 7 or 8 years of age but may become immobile by late adolescence. Seizures severe enough to require hospitalization. Profound to severe ID.
S135P (n=2, S6-S7)	Somewhat small at birth, perinatal difficulties, failure to thrive. Achieve sitting between 19m and 4 years. Seizures may appear after infancy. Severe ID.
S138C (n=2, S8-S9)	Normal to slightly low birthweight, may have feeding difficulties. Mild motor delay (may sit at 10 m), mild speech delay. No seizures. Moderate ID.
T166A (n=4, S10-S13)	Normal birthweight. Mild motor delay at 1 year, mild speech delay (can use complete sentences at 5 years). Seizures likely. May have moderate, mild, or no notable ID. *Exception*: Subject 13 has severe epileptic encephalopathy and severe ID.
G243R (n=2, S14-S15)	Normal birth weight, no neonatal difficulties, but one subject was noted to have developmental delay by the age of 4 months (Subject 14). Acquired growth delay; development slows or regresses, may become nonverbal. Seizures. Severe ID.